TECHNICAL MEMORANDUM

349

Impact of NSCAT winds on tropical cyclones in the ECMWF 4D-Var assimilation system

S. Mark Leidner[1], Lars Isaksen and Ross N. Hoffman

Research Department

[1] Atmospheric Research, Boston, MA, USA

October 2001

European Centre for Medium-Range Weather Forecasts
Europäisches Zentrum für mittelfristige Wettervorhersage
Centre européen pour les prévisions météorologiques à moyen

Series: Technical Memoranda

A full list of ECMWF Publications can be found on our web site under:
http://www.ecmwf.int/publications/

Contact: library@ecmwf.int

European Centre for Medium Range Weather Forecasts
Shinfield Park, Reading, RG2 9AX, England

Abstract

The impact of NASA Scatterometer (NSCAT) data on tropical cyclone forecasting on the European Centre for Medium-Range Weather Forecasts 4-dimensional variational (4D-Var) data assimilation system is examined. Parallel runs with and without NSCAT data were conducted. The 4D-Var can use single level data, such as scatterometer winds, to good advantage. 4D-Var uses data at appropriate times and has the potential to accurately resolve the ambiguity inherent in scatterometer data, by using a two-ambiguity cost function at each NSCAT location. Scatterometer data are shown to improve the depiction of the surface wind field in both tropical cyclones and extratropical lows, and can provide early detection of these features. Case studies of hurricane Lili, and of typhoons Yates and Zane (all in 1996) show major positive impacts of NSCAT data on forecasts of tropical cyclone intensity and position.

1 Introduction

The NASA Scatterometer (NSCAT), aboard the first Advanced Earth Observing Satellite (ADEOS–1), provided high quality ocean surface wind vector data during the nine month ADEOS–1 mission beginning 16 August 1996 (*Freilich and Dunbar* 1999). The focus of this study is the impact of NSCAT data on tropical cyclone forecasting in the European Centre for Medium-Range Weather Forecasts (ECMWF) 4-dimensional variational (4D-Var) data assimilation system. We conducted parallel assimilation experiments with and without NSCAT data. These experiments are denoted "NSCAT" and "NoSCAT" hereafter. In both NSCAT and NoSCAT experiments, winds from the second European Remote Sensing (ERS–2) scatterometer were excluded to highlight the impact of NSCAT. SSM/I wind speed data were also not used, since these data were not available at ECMWF during the periods of the assimilation experiments (1996). Although the NSCAT mission ended prematurely, the follow-on SeaWinds is currently operational aboard the QuikSCAT satellite and has many characteristics in common with NSCAT. Therefore, experience with NSCAT provides useful guidance for the future use of SeaWinds.

A particular concern when using scatterometer wind data is that multiple winds or ambiguities are retrieved at each location (*Price* 1976). The 4D-Var system has the potential to be an accurate ambiguity removal method. Also, 4D-Var uses scatterometer data at the time of each observation, thereby avoiding errors caused by assuming the data are observed at standard synoptic times. Such errors can be significant for quickly evolving surface features, which may be well observed by the scatterometer. The 4D-Var system utilizes two NSCAT wind vector ambiguities at each observation location as described in § 2. Previously, the 4D-Var system has been shown to make good use of European Remote Sensing 1 (ERS–1) scatterometer data for forecasting tropical cyclones (*Isaksen and Stoffelen* 2000). The experiments described here are the first to use NSCAT data in an operational 4D-Var assimilation system. Major positive impacts of NSCAT data on tropical cyclone forecasts are seen in these experiments.

The rest of this section provides some background on scatterometry from satellites, an evaluation of the NSCAT data quality, and a discussion on the impact on global forecast skill scores. In order to explain the lack of impact on these scores, we go into more detail in the succeeding sections and describe the 4D-Var assimilation methodology, our experimental design, case studies of hurricane Lili, and a case study of typhoons Yates and Zane. This paper ends with a discussion of current problems and future opportunities, and some concluding remarks.

1.1 Background

Two principal goals motivated these experiments. First, we wanted to examine the impact of NSCAT in light of the previous study of ERS scatterometer data by *Isaksen and Stoffelen* (2000). Second, we wanted to prepare for SeaWinds, the NSCAT follow-on instrument.

The first satellite to carry a scatterometer was Seasat in 1978 (*Grantham et al.* 1977). When NSCAT was launched, it was the first Ku band ($\sim 14\ GHz$) satellite scatterometer since Seasat (*Naderi et al.* 1991). Since 1991, the European Space Agency (ESA) has flown ERS–1 and ERS–2, which carry an active microwave instrument (AMI) functioning both as a C band ($\sim 5\ GHz$) scatterometer and as a synthetic aperture radar (*Francis et al.* 1991). The ERS data have been used operationally at ECMWF since January 1996, first in 3D-Var as described by *Stoffelen and Anderson* (1997) and currently in 4D-Var as described by *Isaksen and Stoffelen* (2000). Like NSCAT, SeaWinds is also a Ku band scatterometer, but utilizes a very different viewing geometry (*Perry* 2001). The first SeaWinds instrument is now flying on the QuikSCAT satellite. QuikSCAT data has been used experimentally at ECMWF since December 2000, but is not yet used actively. The second SeaWinds instrument is scheduled for launch on ADEOS–2 in February 2002.

Scatterometers measure the backscatter due to the ocean surface roughness via the Bragg scattering mechanism, and thus are most sensitive to centimeter scale waves which are usually in equilibrium with the local wind field. Several measurements of backscatter at a single earth location from different azimuth angles allow the retrieval of near-surface wind vectors. It is not possible to determine a unique solution. Typically two, three or four ambiguous winds will be retrieved (see Fig. 1 middle panel). NSCAT and the other scatterometers mentioned all have/had similar near polar, sun synchronous orbits ($\sim 800\ km$ altitude, $\sim$ 100 minute period). NSCAT had three antennas on each side of the spacecraft, providing coverage in two simultaneous 600 km wide swaths, separated by a 350 km wide nadir gap. All NSCAT observations are avilable at roughly 0600 AM and 0600 PM local time. The fore and aft NSCAT antennas were vertically polarized, and the mid NSCAT antenna was vertically and horizontally polarized. With this geometry, the backscatter values at a single location on the surface are observed from four different azimuth angles within a time span of approximately 70 to 200 seconds, increasing with incidence angle. See the appendix of *Chelton et al.* (2000) for more NSCAT details.

There are several important differences between the wind data sets produced by ERS–1/2 and by NSCAT, which may have a bearing on the impact results. First, the C band radar signal is unaffected by rain, while the Ku band radar signal is both absorbed and scattered by rain, increasingly as the mean drop size grows (*Grassotti et al.* 1999, *Figa and Stoffelen* 2000). Second, ERS–1/2 have antenna only on the right side of the spacecraft. Thus, NSCAT collects measurements over an area roughly twice that of ERS–1 or ERS–2 in the same amount of time. Although the data sampling is 25 km for ERS–1/2 and 50 km for NSCAT, the resolution of all these instruments is effectively 50 km. There is also a 25 km NSCAT near real-time data product, but we use the 50 km NSCAT science data product in this study. Third, ERS–1/2 usually retrieves exactly two ambiguities. Additional wind ambiguities (i.e., more than two) for ERS–1/2 are ignored because the correct ambiguity is almost always the most likely or the next most likely (*Stoffelen and Anderson* 1997). But winds retrieved from NSCAT often have three or four ambiguities, with a primary pair of solutions opposed by 180° and a secondary pair also opposed by 180°. In the case of NSCAT the third or fourth ambiguity is closest to the true wind approximately 5% of the time.

There has been a long history of research on the use of scatterometer data for numerical weather prediction (NWP), which has focussed on evaluating the impact of the data and on developing methods to optimize the use of the data (*Atlas and Hoffman* 2000). Results have been mixed. Early simulation experiments (e.g., *Cane et al.* 1981) tended to be overly optimistic due to various simplifying assumptions which were made. Early real data experiments (e.g., *Anderson et al.* 1991a, 1991b, *Hoffman* 1993) showed very little impact. Single level data like scatterometer winds tend to have little impact in traditional data assimilation systems based on statistical interpolation. More recent studies with ERS–1 and ERS–2 data have shown these data to be valuable in the Southern Hemisphere extratropics and tropics, and on occasion in the North Atlantic and North Pacific. Studies have been conducted by researchers at ECMWF (*Le Meur et al.* 1997, *Andersson et al.* 1998,*Tomassini et al.* 1998, *Isaksen and Stoffelen* 2000), at the NASA Data Assimilation Office (DAO) (*Atlas and Hoffman* 2000), at the United Kingdom Meteorological Office (UKMO) (*Andrews and Bell* 1998), and at the Royal Netherlands Meteorological Institute (KNMI) (*Stoffelen and van Beukering* 1997). Since NSCAT data were never available operationally due to the short lifetime of the satellite, the operational centers have not focussed on these data. The only published NSCAT impact studies to date are those conducted by the DAO (*Atlas et al.* 1999, *Atlas and Hoffman* 2000). The studies examining the combined impact of ERS–1 and ERS–2 at ECMWF and at KNMI and comparing ERS–1 to NSCAT at the DAO suggest that the potential impact of ERS is hampered by its narrow swath width.

Past scatterometer impact studies have been motivated in part by the belief that ocean surface wind data, properly used, *must* be critically important to NWP. The surface wind is the main factor controlling the exchanges of heat, moisture and momentum between the ocean and atmosphere, physical processes which are critical to the energetics of both the ocean and atmosphere. Scatterometer data should be especially useful in 4D-Var systems, which can use single level data to good advantage. For example, *Thépaut et al.* (1993) showed that 4D-Var systems can be extremely sensitive to a single surface wind observation, as well as to scatterometer data. Similar results were found by *Järvinen et al.* (1999). Scatterometer data can improve analyses and forecasts of extreme weather events by enhancing the depiction of the surface wind field for both tropical cyclones and extratropical lows and can provide early detection of these features. For example, *Brown and Zeng* (1994) showed that surface pressure analyses derived from ERS–1 winds capture many details not present in ECMWF operational analyses. Also, *Katsaros et al.* (2001) demonstrated how QuikSCAT's ability to see through upper level cloud facilitated early identification of tropical depressions in the 1999 North Atlantic hurricane season. These examples indicate potential capabilities of scatterometer data for improving NWP in exceptional cases.

In spite of the above arguments suggesting that scatterometer data should significantly impact NWP, the operational centers have been slow to adopt these data. At ECMWF, the operational system is so highly optimized to current data that demonstrating a statistically significant positive impact of a new high quality observing system or an improved assimilation technique requires substantial work (e.g., *Andersson et al.* 1998). For this reason and because we expect the greatest impact of NSCAT data to be on tropical cyclone forecasting, we focus on case studies of particular tropical cyclones. In particular, we examine the impact of assimi-

lation system resolution on the use of NSCAT data and its affect on the analysis and forecast performance.

1.2 Overall evaluation of NSCAT data

Other authors have compared scatterometer winds to ships, buoys, other satellite instruments, and to other forecasts and analyses. Comparisons between scatterometer winds and *in situ* measurements are not without difficulty—the number of collocations with high quality research vessels and buoys is small and there are very significant differences between the space and time scales of the scatterometer and *in situ* measurements. It is often difficult to correct *in situ* observations properly for height and stability effects. *Freilich and Dunbar* (1999) compared NSCAT-1 vector winds with 30 moored National Buoy Data Center buoys, using the methodology of *Freilich* (1997). They found that the Root-Mean-Square (RMS) wind speed difference was 1.3 m/s, and for winds with speeds $> 6\ m/s$, there were very few (~ 3 percent) gross ($> 90°$) ambiguity removal errors. Excluding gross ambiguity removal errors, they found that the directional differences had a mean of 8° (NSCAT clockwise relative to the buoys) and a standard deviation of 17°. *Atlas et al.* (1999) compared NSCAT winds to ships and buoys, SSM/I wind speeds and independent analyses. They report RMS wind speed differences of 2.0 m/s relative to buoys or to the NCEP operational analyses, and 1.4 m/s relative to SSM/I; and RMS wind direction differences of $< 20°$ relative to buoys or to the analyses. For comparison, *Stoffelen* (1998) performed triple collocations of *in situ*, ECMWF forecast and ERS–1 winds with most of the *in situ* observations from NOAA buoys. This analysis showed that ERS–1 is biased low by 4% relative to the *in situ* data, but is more accurate, with standard deviations of wind components for ERS–1 of $\sim 1.75\ m/s$ and for *in situ* data of $\sim 1.95\ m/s$.

Ebuchi and Graber (1998) point out that the distribution of wind speed and direction should be independent of the scatterometer. However, early studies of ERS–1 and NSCAT (using preliminary NSCAT data based on the SASS2 model function) found that histograms of wind direction, relative to antenna direction, showed preferred directions. In a more recent study, using NSCAT winds based on the NSCAT-1 model function, *Ebuchi* (1999) found much improved, physically consistent, histograms of wind speed and direction for varying incidence angles.

We compared NSCAT winds to ECMWF forecasts and analyses. Figure 2 shows that NSCAT winds are in generally good agreement with ECMWF first guess winds. (First guess winds are the product of a 6 h forecast.) This figure shows collocations between ECMWF first guess winds and the closest NSCAT ambiguity over a six day period ($> 750,000$ collocations). There are two notable deviations, however: a small wind speed bias and a small rain contamination signal. ECMWF first guess winds are about 0.63 m/s slower than the NSCAT winds for nearly all wind speeds. There are four factors which contribute to the wind speed bias. First, the scatterometer observes smaller-scale features than are represented by the forecast model at ECMWF (see § 2 for a discussion of the forecast model configuration used in this study). This is especially true for high winds and can be seen in Fig. 2 as an increasing bias for winds $> 15\ m/s$. Second, the NSCAT winds used in this study are the result of wind retrievals using the NSCAT-2 model

function, which was derived in part using ECMWF surface winds. So one would expect the NSCAT winds statistically to agree more closely with the ECMWF model winds because of their dependence. However, the ECMWF forecast model is improved periodically, and the mean surface wind speed in the model changes slightly with time. The ECMWF surface winds are somewhat slower today than in 1996, due to a modified convective parameterization and introduction of a coupled wave model. Thus, NSCAT winds appear to be too fast relative to today's operational system. Since ECMWF surface wind speeds today are closer to buoy observations than in 1996, NSCAT winds may be slightly high. Third, there is some evidence of rain contamination in the NSCAT data in the $0-10\ m/s$ wind speed range from Fig. 2. A small increase in the density of points far above the 45° line indicates high NSCAT wind speeds which may be rain contaminated. Finally, retrieved NSCAT winds assume neutral stability in the boundary layer, and this is a very good approximation over much of the global oceans. But where the boundary layer is stably stratified, the true winds will be less than those in neutral conditions. Therefore, NSCAT winds will overestimate the true wind speed by as much as 15% where the boundary layer is stable. The wind speed bias and its causes are not addressed in this study. We conducted several experiments with wind speed bias corrected NSCAT data (not shown). We found the bias correction had no effect on overall forecast skill or forecast skill with respect to tropical cyclones. Because of NSCAT's shortened mission, methods for detecting rain in NSCAT data were not fully developed and were not available to apply as additional quality controls (QC).

Figure 3 demonstrates that 4D-Var is very effective at drawing the analysis close to the NSCAT data. This typical example shows histograms of wind speed departures from the first guess ($o-b$, upper panel) and the analysis ($o-a$, lower panel). Departures are shown for a 12 h period in the Northern Hemisphere extratropics only (20N–90N). The mean departure is reduced by almost half ($0.818 \rightarrow 0.469\ m/s$) and the RMS of the departures is reduced from $2.22 \rightarrow 1.61\ m/s$. Thus, the NSCAT winds are in good agreement with ECMWF short-range forecasts, and 4D-Var creates analyses that fit the data very well. Now we turn our attention to the overall impact on forecasts.

Figure 4 shows the 500 hPa geopotential height anomaly correlation scores for NSCAT and NoSCAT experiments for twenty-four 10-day forecasts. ECMWF operational forecasts are used as the verifying analyses. The impact in the Northern Hemisphere extratropics is neutral and is negative in the Southern Hemisphere extratropics for forecasts beyond 96 h. The cause of the small impact is unclear. We expect to see the largest (positive) impact in the Southern Hemisphere extratropics where fewer observations are routinely available. Similar investigations using the ECMWF 4D-Var system show a neutral Northern Hemisphere extratropics impact and (small) positive impact in the Southern Hemisphere extratropics for ERS-2 (*Isaksen* 1997) and for SeaWinds/QuikSCAT (H. Hersbach, pers. comm. 2001). Therefore, the current results may be an effect of the particular sample of cases used.

To illustrate the variability in forecast skill from day to day, Fig. 5 shows time series of forecast skill for 5–day forecasts in the Northern and Southern Hemisphere extratropics and the Tropics. Anomaly correlation of 500 hPa geopotential height is used for the extratropics and 850 hPa RMS vector wind error is used in the Tropics. The periods of late September 1996 (typhoons

Yates and Zane) and late October 1996 (hurricane Lili) are shown. While there are differences in mean forecast skill between NSCAT and NoSCAT experiments (Fig. 4), these differences are small compared to the day-to-day variability in forecast skill for either experiment. The NSCAT data produces neither spectacular forecast successes nor failures when evaluated with global measures of forecast skill, such as those presented in Figures 4 and 5. We will show later (§ 4, § 5) that the spatial scale of tropical cyclone related improvements from using scatterometer data is often too small to be captured by global forecast scores.

2 4D-Var assimilation method

The data assimilation system used in this study is the Integrated Forecast System (IFS) cycle 19r1 at ECMWF (*Rabier et al.* 2000, *Mahfouf and Rabier* 2000, *Klinker et al.* 2000). Only aspects of the system of particular relevance to this study will be detailed here.

In the IFS, an incremental 4D-Var approach (*Coutier et al.* 1994) is used to produce the analysis. Observations are used to improve an *a priori* estimate of the current state of the global circulation. Assimilation of observations within the IFS requires several model integrations in different configurations. These configurations use different spectral resolutions to optimize the use of computer resources. We will now give a brief description of the steps involved in creating the 4D-Var analyses for this study.

The assimilation time window for 4D-Var in this study is 6 hours, $\pm$ 3 h around the standard analysis times (0000, 0600, 1200 and 1800 UTC). All experiments are performed with 31 vertical levels (model top at 10 hPa). The first trajectory or "screening run" is simply a 6-h forecast from the first guess (background) field. The 6-h forecast is run at high resolution (T319) using the full non-linear model of the atmosphere. Observation-background differences (innovations) are computed at the appropriate time for all observations presented to 4D-Var. These high resolution $o - b$ differences are inputs to the first minimization. At this stage, gross quality controls are applied to the observations to insure that unreasonable values are not used during the minimization. For NSCAT winds, three gross quality controls are applied following the screening run. NSCAT winds at an observation point are removed from the analysis if any of the following conditions is true:

Background check: If the background wind speed or the NSCAT wind speed is greater than 25 m/s.

Sea ice check: The model sea surface temperature is less than 275 K at the observation point.

Dual winds quality control: If the directions of the two NSCAT wind ambiguities are less than 135° apart. Retrieved winds failing this test are believed to be anomalous.

Minimizations are performed at lower resolution (T63 or T106) because of the computational cost of repeated model integrations over a 6-h period. The minimization seeks a best fit

between the analysis and observations $(a-o)$ and between the analysis and background $(a-b)$ assuming certain observation and background errors and constrained by the atmospheric model to produce a balanced, meteorologically consistent increment fields. The fit to observations is determined by the observation cost function, J_o, the fit to the background by the background cost function, J_b and a gravity wave constraint J_c. Thus, the minimization of J, the total cost function,

$$J = J_b + J_o + J_c$$

determines a simultaneous fit to observations and background. The minimization is performed using an adjoint of the linearized forecast model. J is computed from a linearized version of the non-linear model, the so-called tangent linear model. J_o is summed over all observations at the time of the observations, while J_b is determined by the model state at the start of the time window. Gradients due to changes in the initial state (x_i), $\partial J/\partial x_i$ are computed using the adjoint of the tangent linear model. The values of J and the gradients are calculated repeatedly during the iterative minimization of the linearized cost function. We define this step as the 'inner-loop' of 4D-Var. During the latter part of the minimization, variational QC is applied (*Andersson and Järvinen* 1999) which rejects observations whose $o-a$ departure are too large. We found variational QC to be very useful for rejecting occasional scatterometer wind pairs which are turned 90° to the background flow (see upper right corner of Fig. 24 for an example).

The analysis increments $(a-b)$ from the T63 (or T106) fields are added to the T319 initial conditions. Then, a second high-resolution 6 h forecast is run from these updated initial conditions to provide the basis for a second linearized minimization. The second minimization uses more complete physics than the first and is thus computationally more expensive. Finally, the new increments are again added to the initial conditions, and a final 6-h forecast is run from these updated initial conditions to calculate observation-analysis departures (see the example Fig. 3, middle panel). Fields at the center of the assimilation window ('the analysis') are saved as initial conditions for a medium-range forecast (e.g., 10 days in this study).

In the IFS, NSCAT winds are assimilated differently than the other sources of wind data such as SYNOPs, AIREPs, and buoys, because winds retrieved from NSCAT data always have multiple solutions (ambiguities) at one location. Figure 1 shows an example of the NSCAT retrieval residual as a function of u and v wind components (upper panel), and the corresponding NSCAT ambiguous winds (middle panel). Each wind solution has a known likelihood of being the true wind. These likelihoods are a by-product of the wind retrieval and are present in the data. In the experiments presented here, the most likely wind solution and the solution most nearly opposite in wind direction are presented to the assimilation system. These two winds are used in a two-minima observation operator for scatterometer winds (*Stoffelen and Anderson* 1997):

$$J_o^{scat} = \frac{J_1 J_2}{(J_1^p + J_2^p)^{1/p}} = (J_1^{-p} + J_2^{-p})^p$$

with

$$J_i = (\frac{u_i - u}{\sigma_u})^2 + (\frac{v_i - v}{\sigma_v})^2$$

where u and v are the analyzed wind components; u_i and v_i are the corresponding scatterometer observations; σ_u and σ_v are component observation errors for scatterometer measurements, taken to be 2 m/s for both components; p is an empirical exponent set to 4. The bottom panel of Fig. 1 shows an example of the two wind cost function used in this study. This cost function allows the variational system to resolve the directional ambiguity between two wind vectors in a dynamic way during the assimilation process. Note that when the analyzed wind is close to one of the ambiguous winds, J_o^{scat} is effectively identical to a traditional quadratic cost function, J_i.

3 Design of the NSCAT experiments

Our goal in these experiments is to assess the impact of NSCAT wind data in 4D-Var. Although this is the first time NSCAT data have been used in the IFS, previous work using ERS scatterometer data has shown significant impacts on the analysis and forecast of tropical cyclones (*Isaksen and Stoffelen* 2000). Therefore, we focussed our study on periods when intense tropical cyclones were active.

Two set of experiments were run for the latter halves of October and September 1996. The first experiments are for the period 14–29 October 1996, and hurricane Lili was present in Caribbean and Atlantic basins through the period. The Lili experiment stops on October 20 and resumes October 26. During the gap, NSCAT was turned off, so no NSCAT data are available during this period. The second experiments are for the period 20 Sep–03 October 1996, and typhoons Yates and Zane were present in the western tropical Pacific through the period. NSCAT Level 2.0 Science data (50 km resolution, and based on the NSCAT-2 model function) were used in all experiments. ERS-2 and SSM/I wind speed data were left out of the assimilations in order to make a cleaner investigation of the impact of NSCAT winds. Otherwise, the standard set of observations including TOVS radians data and SATOB cloud motion winds were used.

The experiments are described in Table 1. Only two factors are varied in the experiments: the use of NSCAT data, and resolution of the tangent linear and adjoint model (T63, T106). This makes it possible to clearly investigate the impact of NSCAT data on one hand, and higher resolution increments on the other. The effect of higher resolution increments was examined to test the hypothesis that higher resolution during the minimization would allow a better match of the spatial scales of analysis and observation increments. Also, the scales of motion between Yates and Zane (interacting cyclones) were small enough to require higher resolution to resolve important features of their effects on each other.

4 Hurricane Lili

4.1 Synoptic description

Lili was the most intense Atlantic hurricane during the lifetime of NSCAT. Figure 6 shows the track of hurricane Lili, 14–29 October 1996 and typical NSCAT coverage for a 6 h period. After forming in the Caribbean Sea, Lili moved north over Cuba on 18 October 1996 with an estimated maximum surface wind speed of 44 m/s and surface pressure of 975 hPa before landfall. Lili intensified as it went through the Bahamas on 19 October and reached maximum intensity on 20 October (51 m/s, 960 hPa) east of Bahamas. Then Lili moved slowly towards northeast and east during the next four days, gradually becoming weaker and stalling for a period at about 55W. But on 24 October 1996 it started to intensify again and move faster towards Europe under influence of extratropical weather systems. On 25 October it still had hurricane strength and Lili remained a tropical cyclone until 27 October 1996. It then moved to the east until crossing the coast of Ireland on 28 October. For a more detailed synoptic description see *Pasch and Avila* 1999.

Analysis and forecast impacts for two case studies are presented next. The dates of the cases are 0600 UTC 19 October 1996 and 0000 UTC 26 October 1996 (denoted A and B, respectively, in Fig. 6).

4.2 Analysis and forecast impacts

4.2.1 Case of 19 October 1996

The Lili case was run with the T319/T63 assimilation system. Five days into the experiment (0600 UTC 19 October 1996), Lili had just crossed Cuba. Figure 7 shows first guess and analysis fields of Lili for experiments NoSCAT and NSCAT. In both first guess fields (top panels), Lili is southwest of the observed position and too weak by almost 30 hPa. While current global models cannot simulate the intense pressure gradients and high winds observed in the vicinity of tropical cyclones, much more intense tropical cyclones are produced regularly by higher resolution forecast models at ECMWF than for previous lower resolution systems used in operations (*Serrano* 1997). Lili's weak state in the first guess suggests that recent NSCAT data (i.e., within the last 12-18 hours) had little impact on Lili's intensity. Furthermore, as Lili crossed Cuba, fewer NSCAT data were available to identify its position and intensity. The middle panels of Fig. 7 show the NoSCAT and NSCAT analyses. The NoSCAT analysis is changed very subtly, but in the NSCAT analysis, Lili is broader and the center of circulation has shifted to the northeast, towards the correct position. The mean sea level pressure (MSLP) increments for the NSCAT experiment (bottom right panel) are largest to the northeast (-2.3 hPa), and the central pressure is nearly unchanged. Figure 8 shows the scatterometer data presented to the analysis system in the NSCAT experiment. The central part of Lili was observed by

NSCAT on the right side of this ascending pass (rev 900). The Bahama Islands north of Cuba prevented complete observation of Lili's center, and twenty observations closest to Lili's center were rejected by the analysis system. Three NSCAT observation points close to the center of circulation failed the gross high winds check ($>25\ m/s$), and the rest were rejected by variational QC during the assimilation. Winds to the WNW and north of Lili were observed by NSCAT and used in the analysis. The scale of Lili was expanded (perhaps incorrectly) in the NSCAT analysis by the use of only selected observations, because those observations closest to the center of Lili failed quality control checks in the analysis system. Lili may also have become larger because of the large scale of the analysis increments in 4D-Var.

The analyses presented in Fig. 7 were followed by a 1200 UTC analysis and subsequent forecast. Figure 9 shows the 5-day forecast impact in the NoSCAT and NSCAT experiments. Lili's position and intensity are improved through the whole forecast period (1-5 days) in the NSCAT experiment. The "stall" in Lili's movement is captured much better by NSCAT forecast than NoSCAT. The southern offset of both forecast tracks may be due to poor positioning in the initial conditions of both NSCAT and NoSCAT. Lili in the NSCAT forecast seems to be larger than in NoSCAT and the verifying analysis. This may again be a reflection of the use of structure functions optimized for global data assimilation for the analysis of observations close to a tropical cyclone center.

4.2.2 Case of 26 October 1996

By October 26, Lili was in the central Atlantic and making the transition from a hurricane to an extratropical low. Figure 10 shows the analyses at 0000 UT October 26. (The layout is the same as Fig. 7.) NoSCAT and NSCAT experiments resumed at this time after an NSCAT data blackout, so the first guess fields are the same for both experiments. The T319/T63 assimilation system is not able to represent the intense small scale features of hurricane Lili, but it is clear that the NSCAT analysis demonstrates a large improvement in both position and intensity of Lili. Lili is much too weak in both analyses, but the NSCAT analysis demonstrates a great improvement in position and a modest improvement in intensity. In this dramatic case, increments in MSLP of up to 12 hPa and wind increments as large as 17 m/s can be seen. The impact in this case is unusually large compared to typical impacts around cyclones, because of a large error in position in the first guess (uncommon for the Atlantic) and good coverage of Lili's circulation by NSCAT (see Fig. 11). Consistent with the tropical to extratropical transition is the hint of a front in the strong wind shifts extending to the northeast of Lili's center, a feature clearly observed by NSCAT. Figure 12 shows the availability of other observations in the vicinity of Lili. Cloud contamination eliminates TOVS data in the area of interest, the complex flow pattern results in few cloud motion winds near the center of Lili, and there are only two ships and some aircraft data close by. The NoSCAT analysis clearly demonstrates that these data were too sparse to significantly improve Lili's position or intensity.

The large impact of NSCAT data on Lili near the surface is propagated with substantial effect in the vertical. Figures 13–17 show northwest-southeast cross sections through Lili. The cross

section location is shown in Fig. 12. Wind speeds in the NSCAT experiment (Fig. 13) are increased through nearly the whole troposphere, with a maximum scalar wind speed increment of greater than 10 m/s along this cross-section between $700 - 800$ hPa. This corresponds to a $\sim$50% increase in mid-level wind speeds near the center of Lili. There is even evidence of an eye in the NSCAT wind speed increments at (39N,40W), because smaller increments were produced close to the center of circulation. The NoSCAT wind speed increments demonstrate that some aircraft data were used around the 300 hPa level, but had little effect on Lili's intensity or position.

Increments of vertical velocity through the troposphere (Fig. 14) show that NSCAT data have increased the updrafts in Lili by 5 Pa/s at the 600 hPa level and increased sinking motion in the environment around Lili. Temperature increments for the NoSCAT experiment (Fig. 15) show an isolated impact on the analysis from aircraft observations (-1.0 to $+1.5$ C) at the 300 hPa level. Temperature increments for the NSCAT experiment, however, are larger (-1.5 to $+2.5$ C), and temperature is increased by $1.5 - 2.0$ C throughout nearly the whole troposphere in the vicinity of Lili. Lili is still a warm core system, but note that the temperature increments in Fig. 15 are tilted in the vertical, a feature normally associated with a developing baroclinic system.

Lili's increasingly baroclinic character is also clear from a plan view. Figure 16 shows analyses of 500 hPa temperature and MSLP one day later at 0000 UT October 27 for NoSCAT and NSCAT. These fields are no longer aligned in the vertical, as they would be for a tropical cyclone. The use of NSCAT data has clearly increased Lili's intensity. Also, just northwest of the center of Lili between 45N and 50N, the 500 hPa horizontal temperature gradient is nearly twice as strong in NSCAT as in NoSCAT. As Lili continued to move northeastward, it quickly encountered a strong baroclinic region further to the north. The ensuing interaction strengthened and accelerated Lili towards its eventual landfall in Ireland.

Because 4D-Var optimizes the fit between the model and observations over a 6-h period, a surface wind observation may be just as effective as a temperature or moisture observation for modifying an analysis. Mass and wind fields are coupled together by the dynamics and thermodynamics of the model, and it is clear from the cross sections that scatterometer data are useful for much more than improving the surface winds when used in 4D-Var. For example, cross sections of specific humidity (Fig. 17) show that the NSCAT data have produced increments as large as 3.5 g/kg at 800 hPa. This corresponds to a $\sim$50% increase in moisture at mid-levels.

The analysis impact of NSCAT on Lili persisted for the next 36 h. Figure 18 shows NSCAT-NoSCAT MSLP differences for 6 consecutive analysis times. These plots show that the NSCAT MSLP analyses are 9–15 hPa lower than NoSCAT in the vicinity of Lili. This result is surprising so near Europe, and shows that scatterometer data can make significant impacts even in areas traditionally thought to be well observed.

Lili made landfall in Ireland at 1200 UT 28 October, 60 h after the analysis time examined in detail above. Figure 19 shows the 2-day forecast impact for experiments NoSCAT and NSCAT. The minimum central pressure in the NSCAT experiment is 5 hPa lower than in NoSCAT and

closer to the the verifying analysis. The wind speeds are clearly more intense in the NSCAT experiment, especially in the region south of the low where 25 m/s winds are forecast. In the NoSCAT experiment only 20 m/s winds are forecast.

5 Typhoons Yates and Zane

5.1 Synoptic description

Yates and Zane were North Western Pacific tropical cyclones. Yates was active from 17 September until 3 October 1996. It had typhoon strength winds from 23 September until 1 October and even super typhoon strength (67 m/s maximum wind speed) from 24–29 September. Zane was active from 30 September until 6 October 1996. It had typhoon strength (57 m/s maximum wind speed) from 25 September until 3 October 1996. Yates formed at 7N near the date line, whereas Zane originated farther west near (6N,155E). Figure 20 shows their tracks. There are clear signs of tropical cyclone interaction between Yates and Zane. For example, during the period 25 September to 1 October when both Yates and Zane have reached typhoon strength, the tracks follow a tandem linked movement northward, and then northeastward. *Lander et al.* (1999) have a comprehensive discussion regarding the interaction between Yates and Zane. Figure 18 from their paper shows the interaction between Yates and Zane during the recurving period. Based on satellite images (not shown), it can be seen that the inflow region for Yates is affected by Zane and vice versa.

5.2 Analysis and forecast impacts

The benefits of NSCAT data to analyses and forecasts demonstrated for Lili in § 4.2 are emphasized further by the results for Yates and Zane. Here we focus on the analysis and forecast performance on 26 September 1996, six days into the experiment.

In coarse scale assimilation systems, errors in representing the interaction and boundaries of the flow in the vicinity of two interacting tropical cyclones can often lead to misinterpretation of observations. This difficulty is intensified for the ambiguous scatterometer data. Therefore to investigate the importance of resolution on this case, in addition to the normal resolution assimilation system (T319/T63) used for the Lili cases described above in section § 4.2, we performed an additional assimilation with a higher resolution analysis system (T319/T106). The normal resolution assimilation experiments were performed for the period 20 September–03 October, and the higher resolution experiments were performed for the period 26–29 September 1996 (see Table 1).

5.2.1 Case of 26 September 1996

The northwestern Pacific region generally has few conventional observations. In specific cases like this, even fewer conventional observations are available since ships and aircrafts try to avoid typhoons. Figure 21 (upper panel) shows the few active conventional observations available in the vicinity of both Yates and Zane for the 1200 UTC 26 September assimilation. Within a radius of 500 km, only high level aircraft reports were available. The lower panel of Fig. 21 shows that no TOVS data were available in the region for the 1200 UTC 26 September assimilation. Only cloud motion derived winds from geostationary satellites were available, and none were near Yates and Zane due to difficulties in height assignment and the complex flow in the area.

As in the Lili experiments, ERS-2 scatterometer and SSM/I winds were not used in these assimilation experiments so the only remaining source for near-surface satellite winds is NSCAT data. Figure 22 shows the NSCAT data available to the assimilation system from 1200 UTC 26 September until 0000 UTC 28 September 1996. Due to the satellite orbit, NSCAT data is available at 0000 and 1200 UTC in this region, so NSCAT observes both Yates and Zane well every 12 hours during this period. The plots show the position of Yates and Zane and a subset of the NSCAT wind available to the assimilation. The dots show the full 50 km resolution of the NSCAT data used.

An assimilation experiment similar to the Lili case described in § 4.2 was performed at T63 analysis resolution. Figure 23 shows the first guess, analysis and analysis increment of MSL pressure and 10 m wind fields for NoSCAT and NSCAT, valid 1200 UTC 26 September 1996. The NSCAT data locations are marked as small dots. The first guess fields near Zane (20N,128E) are similar, but the analyzed intensity for Zane is significantly better in NSCAT, with an MSL analysis increment of -6 hPa at the right location. Figure 24 shows NSCAT winds near typhoon Zane at 1200 UTC 26 September 1996. The MSL pressure analysis is overlayed, and the JTWC (The Joint Typhoon Warning Center, Hawaii U.S.A) observed center location is marked with a cross-square. The NoSCAT experiment only has a -2.7 hPa increment to the northeast of Zane resulting in an elongated tropical cyclone. The intensity of Yates (17N,142E) is left almost unchanged in both analyses. The position is improved slightly in the NSCAT assimilation, whereas the NoSCAT analysis leaves Yates unchanged. The observed intensity of Yates is a category 4 typhoon (120 mph wind speed) and Zane is a category 3 typhoon (100 mph wind speed) at 1200 UTC 26 September. The assimilation system is not capable of representing such intense tropical cyclones properly (see discussion in § 4.2), but it is able to represent a tropical cyclone-like feature at the resolution of the assimilation system. In this situation, the NSCAT assimilation is able to improve the analysis of Zane but not of Yates. This results in an overall worse analysis, since the relative intensities of the cyclone pair have been changed, with Zane much stronger than Yates. In fact, a comparison of the forecast evolution from the NoSCAT and NSCAT analyses shows a somewhat poorer medium range NSCAT forecast. Figure 25 shows the NoSCAT and NSCAT 132 h forecasts and the verifying analysis. In the NSCAT forecast Zane is too intense (relative to Yates), overtakes and swallows Yates, and produces a larger scale intense low in the wrong position. On the other hand, in the NoSCAT forecast, Zane is too weak and lags behind the observed track. Even though the

NoSCAT forecast is not a good forecast, it still may have been better to leave Zane unchanged in the NSCAT experiment in this case, rather than change the relative strengths of the two typhoons.

The poor NSCAT forecast in this case is in contrast to the improved analyses and forecasts for the two Lili case studies in § 4.2. The Lili experiments were, as described above, performed with a T63 inner loop resolution, so they show that it is possible to obtain positive impact using NSCAT data even with a coarse analysis resolution. Often the analyses of tropical cyclones are improved because the inflow in the surrounding area is described better by the NSCAT data and this helps to improve the general description of the cyclone. Even in the Lili cases in which we observed positive impacts, we typically saw many NSCAT data rejected by the analysis system near the center of the topcial cyclones. Therefore to investigate the importance of inner loop resolution on the use of the NSCAT data, we performed parallel assimilation experiments using T106 resolution. They will be referred to hereafter as NoSCAT106 and NSCAT106.

Figure 26 shows the T106 analyses for NoSCAT106 and NSCAT106 at 1200 UTC 26 September 1996, twelve hours into the assimilation experiment. The two first guess fields are virtually identical in the area of interest. Zane has a central pressure of 1001 hPa, and Yates is 1003 hPa. This is left almost unchanged by the NoSCAT106 analysis, whereas the NSCAT106 analysis intensifies Zane by 6 hPa and moves and intensifies Yates by 4 hPa. The resulting NSCAT106 analysis is the best of the four analyses presented here.

We will now compare the results of the T106 experiment with the T63 experiment around Zane. Figure 27 shows NSCAT data rejection around Zane in T63 and T106 analyses. In the NSCAT experiment, twenty NSCAT observations were removed from the analysis by 4D-Var QC. But only seventeen were removed from the NSCAT106 analysis. The three additional observations accepted by NSCAT106 are just to the south and southeast of the center of Zane (highlighted in the upper panel of Fig. 27). High wind speeds and small spatial scales near the center of a tropical cyclone make these observations very important for improving placement and intensity in the analysis. These three observations alone move Zane $\sim$20 km west (closer to the observed position) and lower the central pressure by $\sim$1 hPa. While this is a modest improvement, it is only attributable to an increase in the resolution of the analysis and clearly shows an improved use of the data.

The 4D-Var assimilation system is capable of propagating information from surface observations throughout the troposphere in a dynamically consistent way. This enhances the impact of NSCAT surface winds. In § 4.2 we presented vertical cross-section examples of Lili, and here, Figs. 28–31 show southwest-to-northeast cross sections of first guess and analysis increment fields through typhoon Zane on 1200 UTC September 1996. The cross section location is shown in Fig. 21. Figure 28 shows the cross-section of the scalar wind speed. The first guess fields are very similar because the assimilations started from identical background fields at 0000 UTC 26 September 1996. The use of NSCAT data introduces a much more intense and balanced tropical cyclone in the NSCAT106 analysis: in the southwestern (left part of the figure) wind speed increments of 8 m/s are seen in NSCAT106 versus only 2 m/s in the NoSCAT106 assimilation. The center of the typhoon is also well defined in the NSCAT106 wind speed increments. 4D-

Var's ability to propagate surface wind information throughout the troposphere is clearly seen in this example where the NSCAT106 increments refine the location of the center of the typhoon, maintaining a tropical cyclone like structure throughout the troposphere. Note the barotropic (untilted) pattern of the increments which have the effect of moving the entire typhoon towards the northeast, very close to the correct location.

Because 4D-Var is a multi-variate analysis with a dynamic forecast model constraint, surface wind observations produce analysis increments for other prognostic variables. In Fig. 29 we show the cross-section of vertical velocity. The pattern in the first guess is amplified by NSCAT data, and only slightly changed in the NoSCAT106 analysis by rawinsonde and aircraft reports in the area (see Fig. 21). Figures 30 and 31 show cross-sections of potential temperature and specific humidity increments, respectively. The potential temperature cross-section shows how a warm core increment is introduced in the lower half of the troposphere near the center of the tropical cyclone. Other observations (in this case aircraft data near the 500 hPa level in Fig. 30, lower right panel) are responsible for some of the temperature increments in the north east region. The NSCAT106 increments that can be attributed to NSCAT data clearly show a "barotropic like" structure for the wind and temperature, as would be expected for a tropical cyclone still at 20N. It is interesting to compare this "barotropic like" cross-section structure for Zane (see Fig. 28) to the more "baroclinic" structure for Lili in Fig. 15, where Lili was becoming an extratropical disturbance in the baroclinic region near 40N. The vertical cross-sections for the equivalent T63 assimilation (not shown) share the same patterns but have, as one would expect, a broader structure than the T106 increments. This is also clear when comparing the Lili T63 case (Fig. 13 has cross-section horizontal length of 2800 km) with the Zane T106 case (Fig. 28 has a cross-section length of 1700 km): the latter covers a much smaller horizontal area.

Figure 32 top and bottom panels show the 132 h NoSCAT106 and NSCAT106 forecasts starting from the analyses of Fig. 26. The verifying analysis is shown in the middle panel. The NoSCAT forecast is very similar to the T63 forecast presented in Fig. 25 (bottom panel) with Zane much weaker than Yates, with too large a distance between the two storms. The NSCAT106 forecast is substantially better than the NSCAT forecast for this case—the forecast position and intensities of both Yates and Zane are improved. Recall, in the NSCAT forecast, Yates and Zane merge. Here, in the NSCAT106 experiment, the separation and intensity of the storms are more correctly forecast. This case is also an example that shows the importance of treating tropical cyclones properly when they start to interact with the extratropical flow. In Fig. 33, the 500 hPa anomaly correlation scores for the north Pacific show how the general circulation of the region was dramatically improved during the first days of October (i.e., in the 4-5 day forecast range) in the NSCAT106 experiment compared to the NSCAT experiment. Notice that the NoSCAT106 experiment is also improved over the NoSCAT experiment, but not as much as the improvement from NSCAT to NSCAT106. The improvement in the NSCAT106 experiment can be attributed to higher resolution analysis increments which leads to improved use of the data. It is only in a dramatic situation like this where one would expect to see such a marked impact of NSCAT data.

We can conclude that the complexity of the two interacting typhoons requires T106 analysis

resolution to use the NSCAT data properly, and that higher resolution analyses make better use of NSCAT data.

6 Current issues and the future

There are a number of issues which could improve the use of NSCAT data, and which have a bearing on the use of SeaWinds data for NWP. Anticipated improvements in the 4D-Var data assimilation system and/or improvements in the scatterometer data are expected to resolve each of the following issues in the next several years.

- Higher spatial coverage due to wider swaths, or multiple instruments increases the effect of scatterometer data. Data coverage increases approximately by a factor of two from ERS–2 to NSCAT to SeaWinds. Also, two SeaWindsinstruments should be operational after the launch of ADEOS–2, and the double swath C-band ASCAT instrument on METOP-1 will replace ERS-2. The wider swaths of SeaWinds should result in fewer circulation centers just beyond the swath edges such as Yates in the lower right panel of Fig. 22.

- Ku band scatterometers are affected by rain. Special quality control (QC) or correction for rain effects may be important. In the present study we ignored rain, but the QC procedures in the data assimilation system eliminate the worst scatterometer wind observations. QuikSCAT data seems to be more sensitive to rain, but has a number of QC flags which are useful for data screening. SeaWinds on ADEOS–2 will be accompanied by an Advanced Microwave Scanning Radiometer (AMSR), which will allow precise rain QC, and which may allow the SeaWinds backscatter observations to be corrected for rain effects.

- Although 4D-Var makes use of a two-wind scatterometer cost function and all other *a priori* data when resolving the ambiguity in the scatterometer winds, if the location of an intense feature in the background has a substantial error, the wrong ambiguity will be in agreement with the background, and may therefore be used. Wider swaths may alleviate this problem. In addition the methodology of *Hoffman et al.* (1995) could be used to align features present in the background and observations.

- When the scatterometer winds are in error due to rain contamination or ambiguity removal errors, it is likely that patches of data will be affected. The 4D-Var can explicitly account for horizontal observational error correlations or the estimated observation errors can be inflated so as to deweight correlated data.

- Higher (inner loop) resolution of the 4D-Var will allow the analysis of smaller scales of motion, scales present in the full model and in the scatterometer data, but which are currently filtered by 4D-Var minimization. An updated background error covariance matrix would also improve the use of scatterometer data on smaller scales.

- Longer cycling window for the 4D-Var (say 12 hours instead of 6 hours) will allow for more physically consistent use of the scatterometer data, and greater influence on upper levels . This is partly because the analysis is forced to fit more scatterometer orbits in a consistent flow dependent way. However, a longer cycling window may violate the 4D-Var assumption that model errors are negligible compromising the quality of innovations and the model trajectory.
- Refined observation cost functions for scatterometer data may enhance the impact of these data. For example it is possible to directly use the backscatter data (*Thépaut et al.* 1993). Alternatively, it should be possible to formulate cost functions in terms of the wind ambiguities which more closely reflect the backscatter cost function used to retrieve the ambiguities.

7 Conclusions

We examined the impact of NSCAT data on tropical cyclone forecasting on the ECMWF 4D-Var data assimilation system. Although the NSCAT mission ended prematurely, the follow-on SeaWinds instrument aboard the QuikSCAT satellite is currently operational, and experience with NSCAT provides useful guidance for SeaWinds. We conducted parallel runs denoted NSCAT and NoSCAT, with and without NSCAT data, respectively. In the NSCAT experiments, 4D-Var is presented with two ambiguities and effectively resolves the ambiguity using a special cost function. This paper has concentrated on evaluating the impact of NSCAT data on tropical cyclones by highlighting a few typical examples. In general NSCAT data is expected to improve the surface wind fields, especially in the tropics and southern hemisphere, leading to improved surface fluxes. These effects cannot be quantified in the relatively short assimilation experiments we have conducted. Similarly it is not possible to evaluate the impacts on overall skill scores because of the small sample. Even small improvements in forecast skill are hard to come by in current state-of-the-science data assimilation systems like the ECMWF 4D-Var. However, case studies of hurricane Lili, and of typhoons Yates and Zane show major positive impacts of NSCAT data on tropical cyclone forecasts of both intensity and position. This is a significant result but not unexpected: scatterometer data have previously been shown to improve the depiction of the surface wind field in both tropical cyclones and extratropical lows, and can provide early detection of these features. Additionally in the 4D-Var, scatterometer observations are assimilated properly in time and space, and the dynamics of 4D-Var allows the influence of surface observations to be propagated more correctly in the vertical.

Specific notable impacts include:

- improved 2–5 day forecast tracks of tropical cyclones
- better analyzed thermodynamic structure of tropical cyclones via 4D-Var
- improved use of NSCAT winds using higher resolution (T106) analysis increments

- improved representation of binary tropical cyclone systems using higher resolution (T106) analysis increments

- consistent and remarkably large increments for all model variables attributable solely to NSCAT data. The largest increments linked to NSCAT data are of the same magnitude as the first guess field values for horizontal wind speed and vertical velocity. For temperature, increments of 1-2 C are common throughout the troposphere, and for specific humidity, the increment magnitude is 10-40 % of the background field values.

8 Acknowledgments

This research was supported by the NSCAT and SeaWinds NASA scatterometer projects and ESA/ESTEC project ref. 111699/95/NL/CN. This work was carried out while the first author was a visiting scientist at the European Centre for Medium-Range Weather Forecasts (ECMWF). We thank ECMWF for generous facilities and administrative support. We thank the NASA Physical Oceanography Data Active Archive Center (PODACC) for supplying the NSCAT data.

References

[1] D. Anderson, A. Hollingsworth, S. Uppala, and P. Woiceshyn. A study of the use of scatterometer data in the European Centre for Medium-range Weather Forecasts operational analysis-forecast model. 1. Quality assurance and validation. *J. Geophys. Res.*, 96(C2):2619–2634, 1991.

[2] D. Anderson, A. Hollingsworth, S. Uppala, and P. Woiceshyn. A study of the use of scatterometer data in the European Centre for Medium-range Weather Forecasts operational analysis-forecast model. 2. Data impact. *J. Geophys. Res.*, 96(C2):2635–2647, 1991.

[3] E. Andersson, J. Haseler, P. Undén, P. Courtier, G. Kelly, D. Vasiljevic, C. Brankovic, C. Cardinali, C. Gaffard, A. Hollingsworth, C. Jakob, P. Janssen, E. Klinker, A. Lanzinger, M. Miller, F. Rabier, A. Simmons, B. Strauss, J.-N. Thépaut, and P. Viterbo. The ECMWF implementation of three-dimensional variational assimilation (3D-Var). III: Experimental results. *Quart. J. Roy. Meteor. Soc.*, 124(550):1831–1860, July (Part B) 1998.

[4] E. Andersson and H. Järvinen. Variational quality control. *Quart. J. Roy. Meteor. Soc.*, 125(554):697–722, Jan. (Part B) 1999.

[5] P. L. Andrews and R. S. Bell. Optimizing the United Kingdom Meteorological Office data assimilation for ERS-1 scatterometer winds. *Mon. Wea. Rev.*, 126(3):736–746, Mar. 1998.

[6] R. Atlas, S. C. Bloom, R. N. Hoffman, E. Brin, J. Ardizzone, J. Terry, D. Bungato, and J. C. Jusem. Geophysical validation of NSCAT winds using atmospheric data and analyses. *J. Geophys. Res.*, 104(C5):11405–11424, 15 May 1999.

[7] R. Atlas and R. N. Hoffman. The use of satellite surface wind data to improve weather analysis and forecasting. In D. Halpern, editor, *Satellites, Oceanography and Society*, Elsevier Oceanography Series 63, pages 57–78, Lisbon, Portugal, 2000. Elsevier, Amsterdam, the Netherlands. ISBN 0-444-50501-6.

[8] R. A. Brown and L. Zeng. Estimating central pressures of oceanic mid-latitude cyclones. *J. Appl. Meteor.*, 33(9):1088–1095, Sept. 1994.

[9] M. A. Cane, V. J. Cardone, M. Halem, and I. Halberstam. On the sensitivity of numerical weather prediction to remotely sensed marine surface wind data: A simulation study. *J. Geophys. Res.*, 86(C9):8093–8106, 1981.

[10] D. B. Chelton, M. H. Freilich, and S. K. Esbensen. Satellite observations of the wind jets off the Pacific coast of Central America. Part I: Case studies and statistical characteristics. *Mon. Wea. Rev.*, 128(7):1993–2018, July 2000.

[11] P. Courtier, J.-N. Thépaut, and A. Hollingsworth. A strategy for operational implementation of 4D-Var, using an incremental approach. *Quart. J. Roy. Meteor. Soc.*, 120:1367–1387, 1994.

[12] N. Ebuchi. Statistical distribution of wind speeds and directions globally observed by NSCAT. *J. Geophys. Res.*, 104(C5):11393–11403, 15 May 1999.

[13] N. Ebuchi and H. C. Graber. Directivity of wind vectors derived from the ERS-1/AMI scatterometer. *J. Geophys. Res.*, 103(C4):7787–7797, 15 Apr. 1998.

[14] J. Figa and A. Stoffelen. On the assimilation of Ku-band scatterometer winds for weather analysis and forecasting. *IEEE Trans. Geosci. Remote Sens.*, 38(4):1893–1902, July 2000.

[15] R. Francis, G. Graf, P. G. Edwards, M. McCaig, C. McCarthy, P. Dubock, A. Lefebvre, B. Pieper, P.-Y. Pouvreau, R. Wall, F. Wechsler, J. Louet, and R. Zobl. The ERS-1 spacecraft and its payload. *ESA Bulletin*, (65):27–48, Feb. 1991. ERS-1 Special Issue.

[16] M. H. Freilich. Validation of vector magnitude datasets: Effects of random component errors. *J. Atmos. Ocean. Technol.*, 14(3):695–703, June 1997.

[17] M. H. Freilich and R. S. Dunbar. The accuracy of the NSCAT 1 vector winds: Comparisons with National Data Buoy Center buoys. *J. Geophys. Res.*, 104(C5):11231–11246, 15 May 1999.

[18] W. L. Grantham, E. M. Bracalente, W. L. Jones, and J. W. Johnson. The Seasat-A satellite scatterometer. *IEEE J. Oc. Eng.*, OE-2:200–206, 1977.

[19] C. Grassotti, S. M. Leidner, J.-F. Louis, and R. N. Hoffman. Development and application of a visible-infrared rain flag for scatterometer data. *J. Appl. Meteor.*, 38(6):665–676, June 1999.

[20] R. N. Hoffman. A preliminary study of the impact of the ERS 1 *C*-band scatterometer wind data on the ECMWF global data assimilation system. *J. Geophys. Res.*, 98(C6):10233–10244, 1993.

[21] R. N. Hoffman, Z. Liu, J.-F. Louis, and C. Grassotti. Distortion representation of forecast errors. *Mon. Wea. Rev.*, 123(9):2758–2770, Sept. 1995.

[22] L. Isaksen. Impact of ers scatterometer data in the ecmwf 4d-var assimilation system. preliminary studies. In *Space at the Service of our Environment*, pages 1829–1851, Florence, Italy, May 1997. ESTEC, European Space Agency. [SP-414] Available from ESA Publications Division, ESTEC Noordwijk, The Netherlands.

[23] L. Isaksen and A. Stoffelen. ERS scatterometer wind data impact on ECMWF's tropical cyclone forecasts. *IEEE Trans. Geosci. Remote Sens.*, 38(4):1885–1892, July 2000.

[24] H. Järvinen, E. Andersson, and F. Bouttier. Variational assimilation of time sequences of surface observations with serially correlated errors. *Tellus*, 51A:469–488, 1999.

[25] K. B. Katsaros, E. B. Forde, P. Chang, and W. T. Liu. QuikSCAT's SeaWinds facilitates early identification of tropical depressions in 1999 hurricane season. *Geophys. Res. Lett.*, 28(6):1043–1046, 15 Mar. 2001.

[26] E. Klinker, F. Rabier, G. Kelly, and J.-F. Mahfouf. The ECMWF operational implementation of four-dimensional variational assimilation. III: Experimental results and diagnostics with operational configuration. *Quart. J. Roy. Meteor. Soc.*, 126(564):1191–1215, Apr. (Part A) 2000.

[27] M. A. Lander, E. J. Trehubenko, and C. P. Guard. Eastern hemisphere tropical cyclones of 1996. *Mon. Wea. Rev.*, 127(6):1274–1300, June 1999.

[28] D. Le Meur, L. Isaksen, B. Hansen, R. Saunders, and P. Janssen. Global validation of ERS wind and wave products. Final Report, European Space Agency, 1997. 256 pages. [Contract 8488/95/NL/CN] Available from ESA Publications Division, ESTEC Noordwijk, The Netherlands.

[29] J.-F. Mahfouf and F. Rabier. The ECMWF operational implementation of four-dimensional variational assimilation. II: Experimental results with improved physics. *Quart. J. Roy. Meteor. Soc.*, 126(564):1171–1190, Apr. (Part A) 2000.

[30] F. M. Naderi, M. H. Freilich, and D. G. Long. Spaceborne radar measurement of wind velocity over the ocean—an overview of the NSCAT scatterometer system. *Proc. IEEE*, 79:850–866, 1991.

[31] R. J. Pasch and L. A. Avila. Atlantic hurricanes of 1996. *Mon. Wea. Rev.*, 127(5):581–610, May 1999.

[32] K. L. Perry. QuikSCAT science data product user's manual, overview and geophysical data products. Version 2.1, Jet Propulsion Laboratory, Pasadena, CA, Apr. 2001. [JPL D-18053].

[33] J. C. Price. The nature of multiple solutions for surface wind speed over the oceans from scatterometer measurements. *Remote Sens. Environ.*, 5:47–54, 1976.

[34] F. Rabier, H. Järvinen, E. Klinker, J.-F. Mahfouf, and A. Simmons. The ECMWF operational implementation of four-dimensional variational assimilation. I: Experimental results with simplified physics. *Quart. J. Roy. Meteor. Soc.*, 126(564):1143–1170, Apr. (Part A) 2000.

[35] E. Serrano. Tropical cyclones. Re-Analysis Project Report Series 5, ECMWF, Reading, U.K., 1997. 30 pages.

[36] A. Stoffelen. Toward the true near-surface wind speed: Error modeling and calibration using triple collocation. *J. Geophys. Res.*, 103(C4):7755–7766, 15 Apr. 1998.

[37] A. Stoffelen and D. Anderson. Ambiguity removal and assimilation of scatterometer data. *Quart. J. Roy. Meteor. Soc.*, 123(538):491–518, Jan. (Part B) 1997.

[38] A. Stoffelen and P. van Beukering. Implementation of improved ERS scatterometer data processing and its impact on HIRLAM short range weather forecasts. HIRLAM Technical Report 31, Irish Meteorological Service, Dublin, Ireland, 1997. 77 pages.

[39] J.-N. Thépaut, R. N. Hoffman, and P. Courtier. Interactions of dynamics and observations in a four-dimensional variational assimilation. *Mon. Wea. Rev.*, 121:3393–3414, 1993.

[40] M. Tomassini, D. LeMeur, and R. W. Saunders. Near-surface satellite wind observations of hurricanes and their impact on ECMWF model analyses and forecasts. *Mon. Wea. Rev.*, 126(5):1274–1286, May 1998.

9 Tables

Table 1: Experimental design.

Experiment mnemonic	NSCAT data used?	Spectral res. of increments	Data assim. periods	Days of assim.
NoSCAT	No	T63	Sep 1996 (T. Yates/Zane) Oct 1996 (H. Lili)	14 11
NSCAT	Yes	T63	Sep 1996 (T. Yates/Zane) Oct 1996 (H. Lili)	14 11
NoSCAT106	No	T106	Sep 1996 (T. Yates/Zane)	4
NSCAT106	Yes	T106	Sep 1996 (T. Yates/Zane)	4

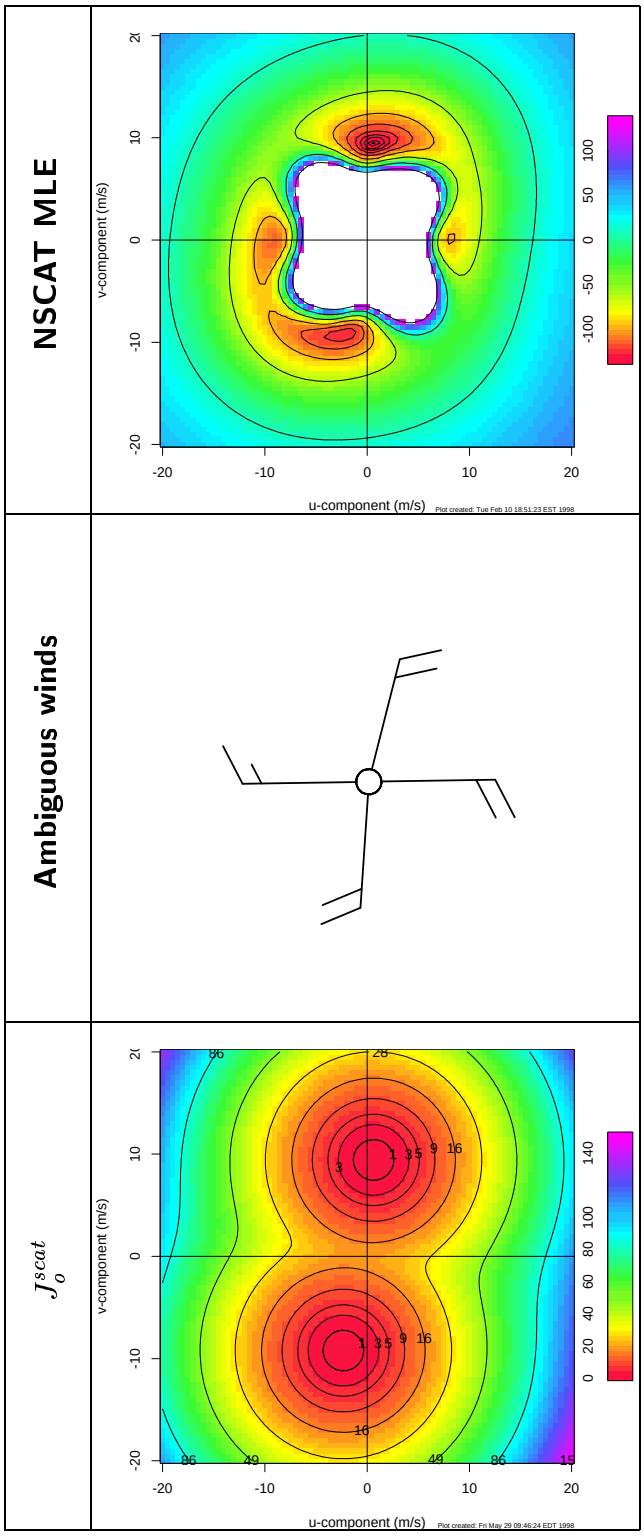

Figure 1: Top panel: plot of Maximum Likelihood Estimator (MLE) for one wind vector cell as a function of u- and v-wind components. Middle panel: ambiguous NSCAT winds corresponding to the top panel. Bottom panel: two-wind cost function used in 4D-Var.

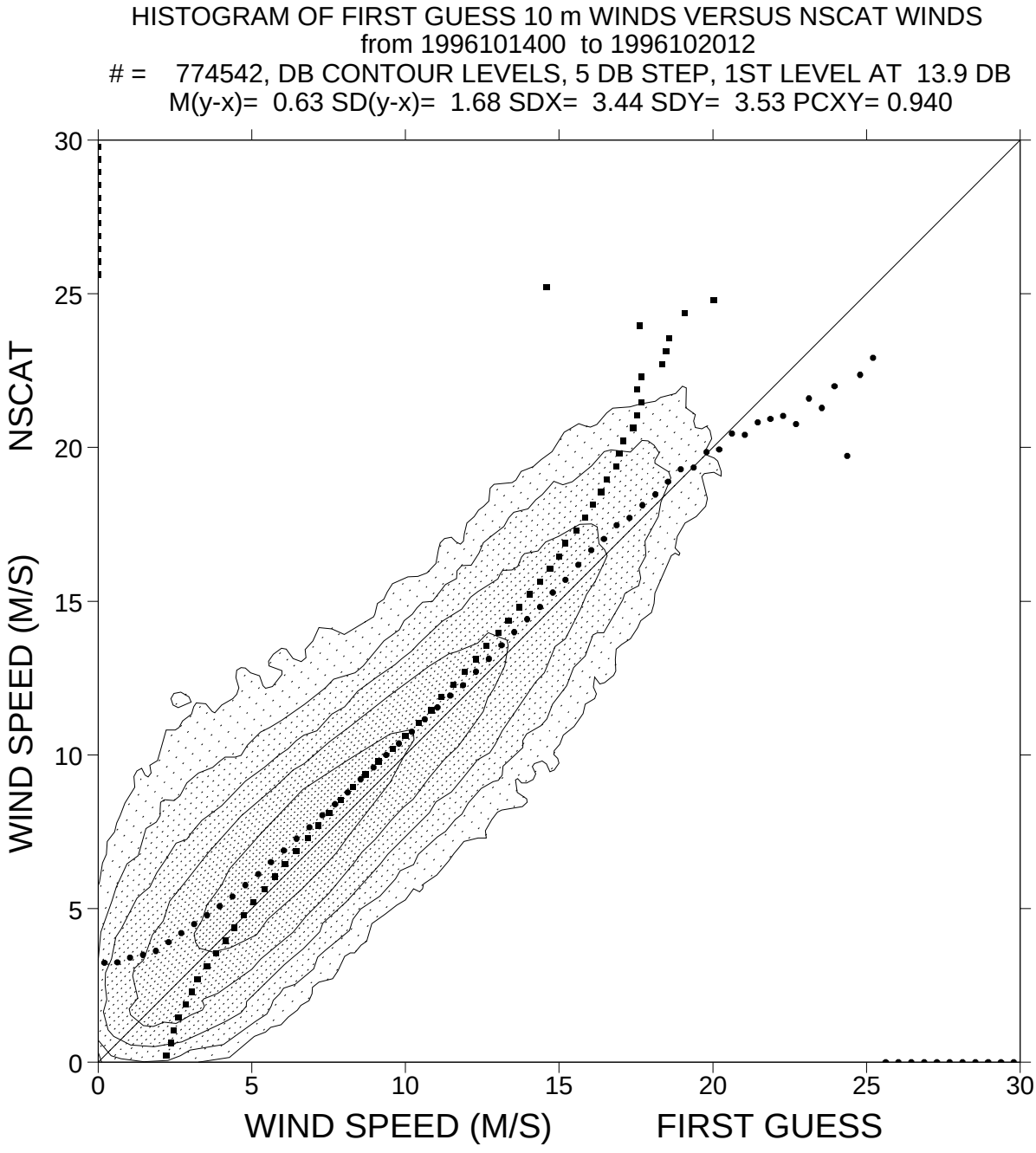

Figure 2: Two-dimensional histogram of NSCAT versus ECMWF first guess winds from the first six days of the Lili NSCAT experiment, 0000 UTC 14 October - 1200 UTC 20 October 1996. The NSCAT ambiguity closest to the first guess field is used for the comparison.

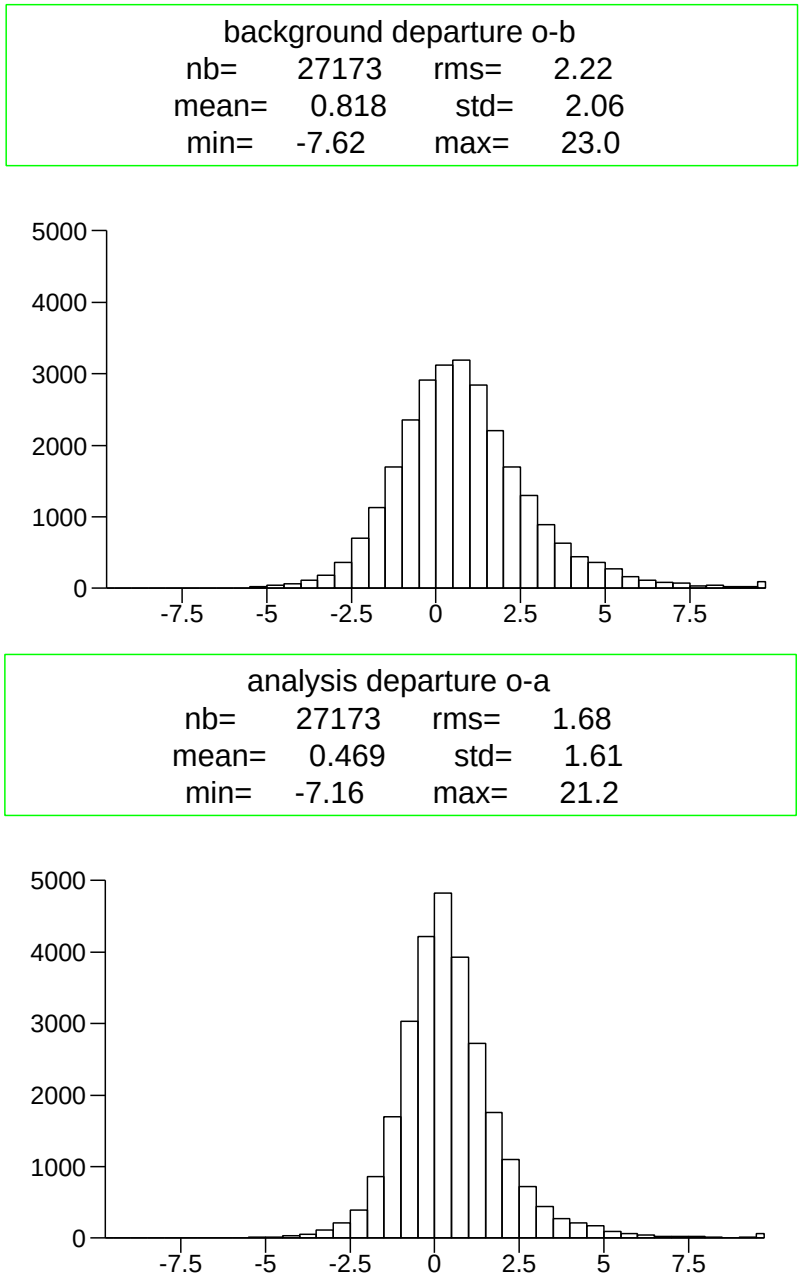

Figure 3: Histograms of wind speed departures of observations from ECMWF first guess winds ($o - b$; upper graph) and ECMWF analyzed winds ($o - a$; lower graph). These departures are for NSCAT data in the Northern Hemisphere extratropics only (20N–90N) for the period 2100 UTC 15 October–0900 UTC 16 October 1996 (from two assimilation cycles).

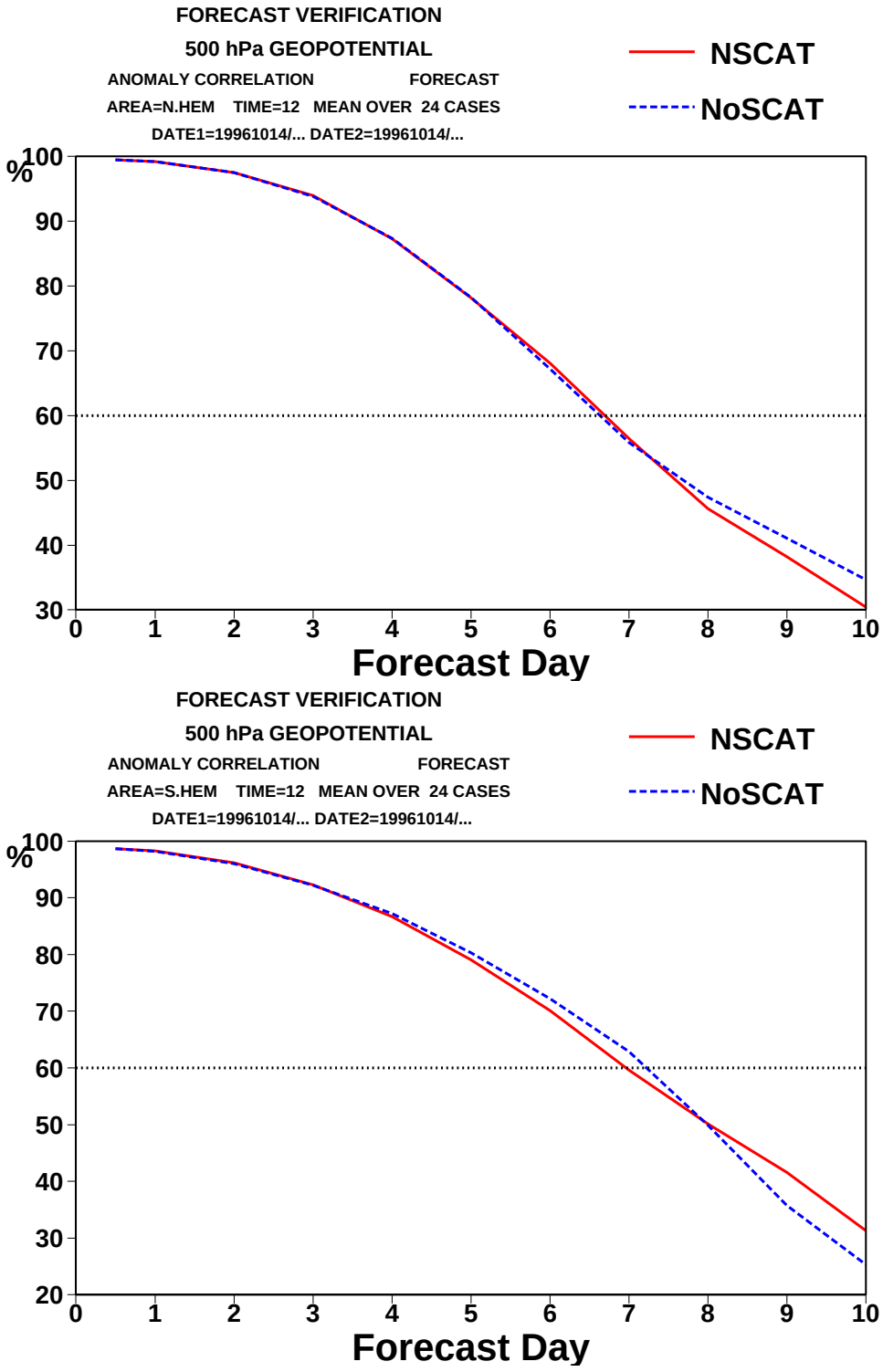

Figure 4: Anomaly correlation scores of Northern Hemisphere extratropics (20N-90N) 500 hPa heights (upper panel), and Southern Hemisphere extratropics (20S-90S) 500 hPa heights (lower panel) for NoSCAT and NSCAT. Scores are computed by comparing each experiment to ECMWF operational analyses.

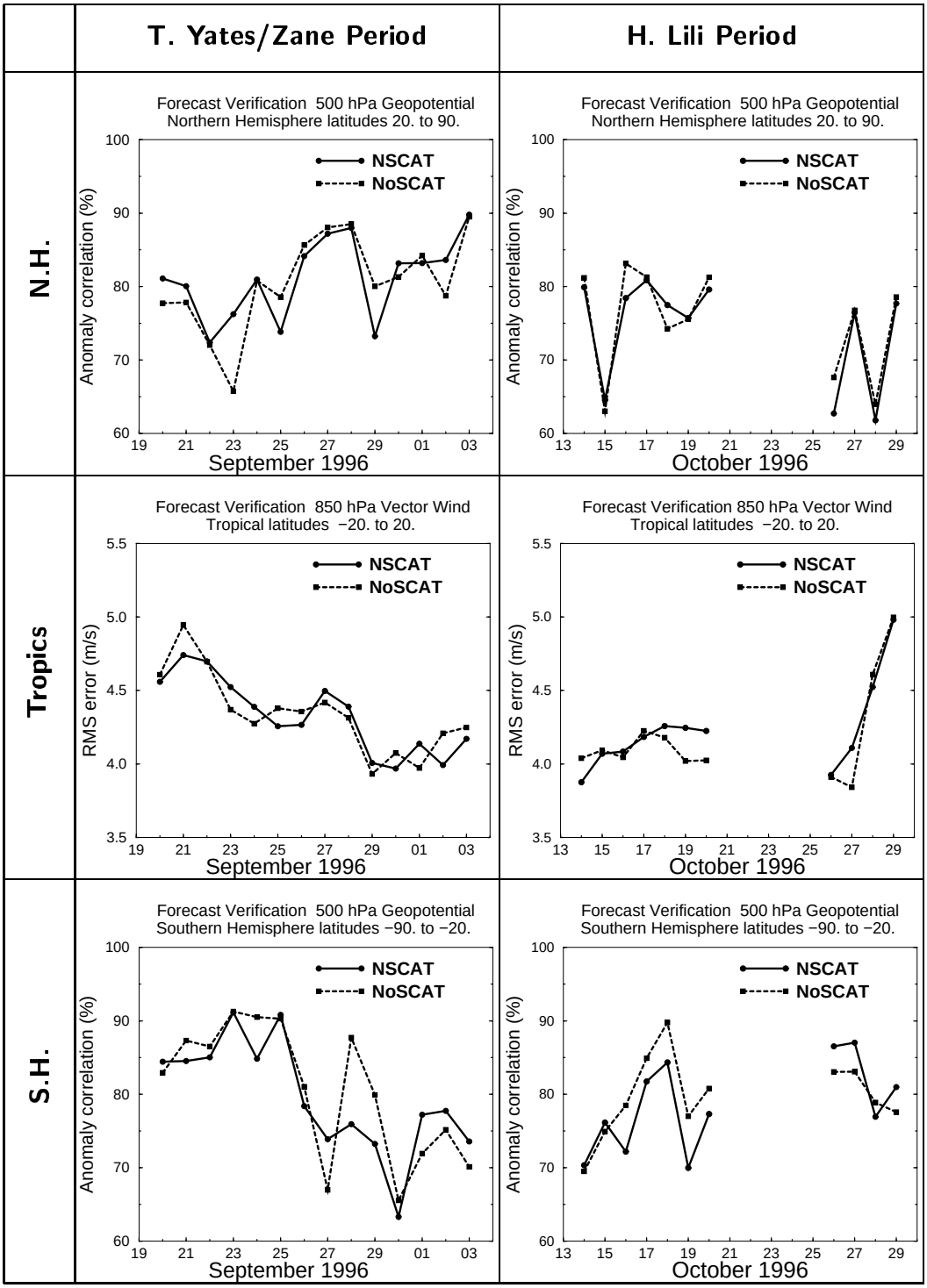

Figure 5: Time series of 5-day forecast scores for NoSCAT and NSCAT experiments for both periods in this study. In the Northern and Southern Hemispheres, the scores are 500 hPa height anomaly correlation. In the Tropics, the scores are 850 hPa vector wind RMS errors.

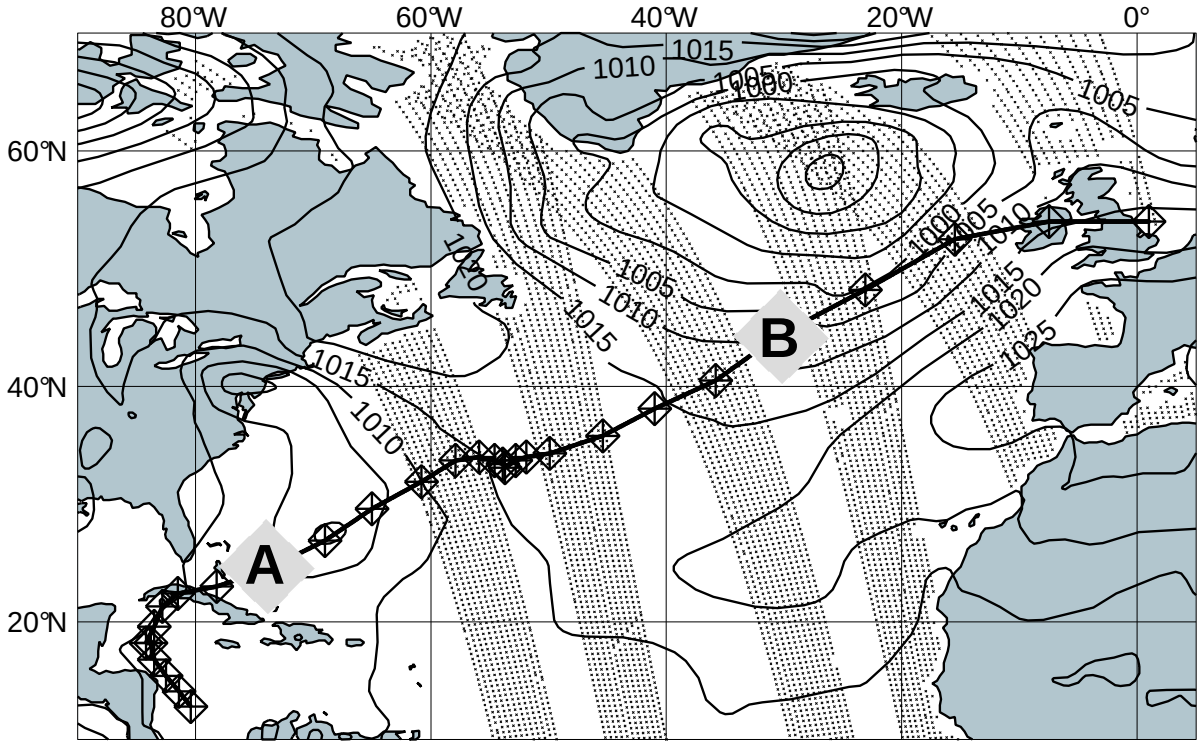

Figure 6: Track of hurricane Lili from 1200 UTC 14 October 1996 to 0000 UTC 29 October 1996. Observed positions at 0000 and 1200 UTC from the National Hurricane Center (NHC) are plotted as diamond-plus symbols along the track. Mean sea-level pressure is valid at 0000 UTC 20 October 1996. Six hour NSCAT data coverage beginning at 2100 UTC 19 October 1996 is shown in fine dots. The observed central pressure and position from the NHC at 0000 UTC 20 October was 964 hPa at 26.9N,69.0W. "A" and "B" mark the positions of Lili at 0600 UTC 19 October and 0000 UTC 26 October 1996, respectively, the two times used as case studies in this paper.

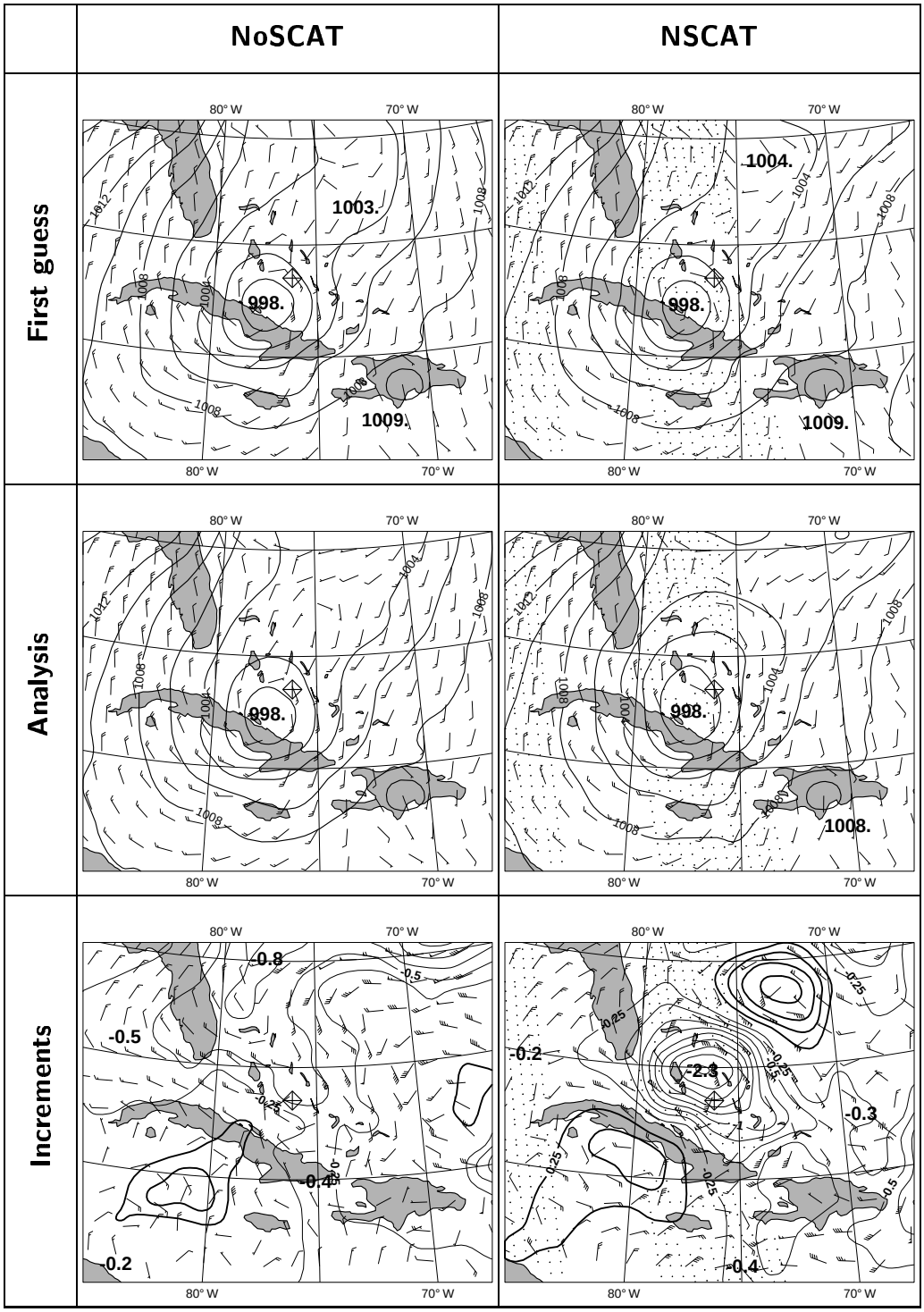

Figure 7: Analysis of Lili 0600 UTC 19 October 1996. Top panels are first guess 10 m wind (knots) and mean sea-level pressure (MSLP, hPa). Middle panels show analyzed wind and MSLP, and bottom panels show analysis increments of wind (times ten) and MSLP. The observed central pressure and position from the NHC at 0600 UTC 19 October was 970 hPa at 23.5N and 76.2W. The observed position is marked in each panel by a diamond-plus symbol. MSLP contour intervals are 2 hPa for first guess and analysis panels, and 0.25 hPa for increment panels.

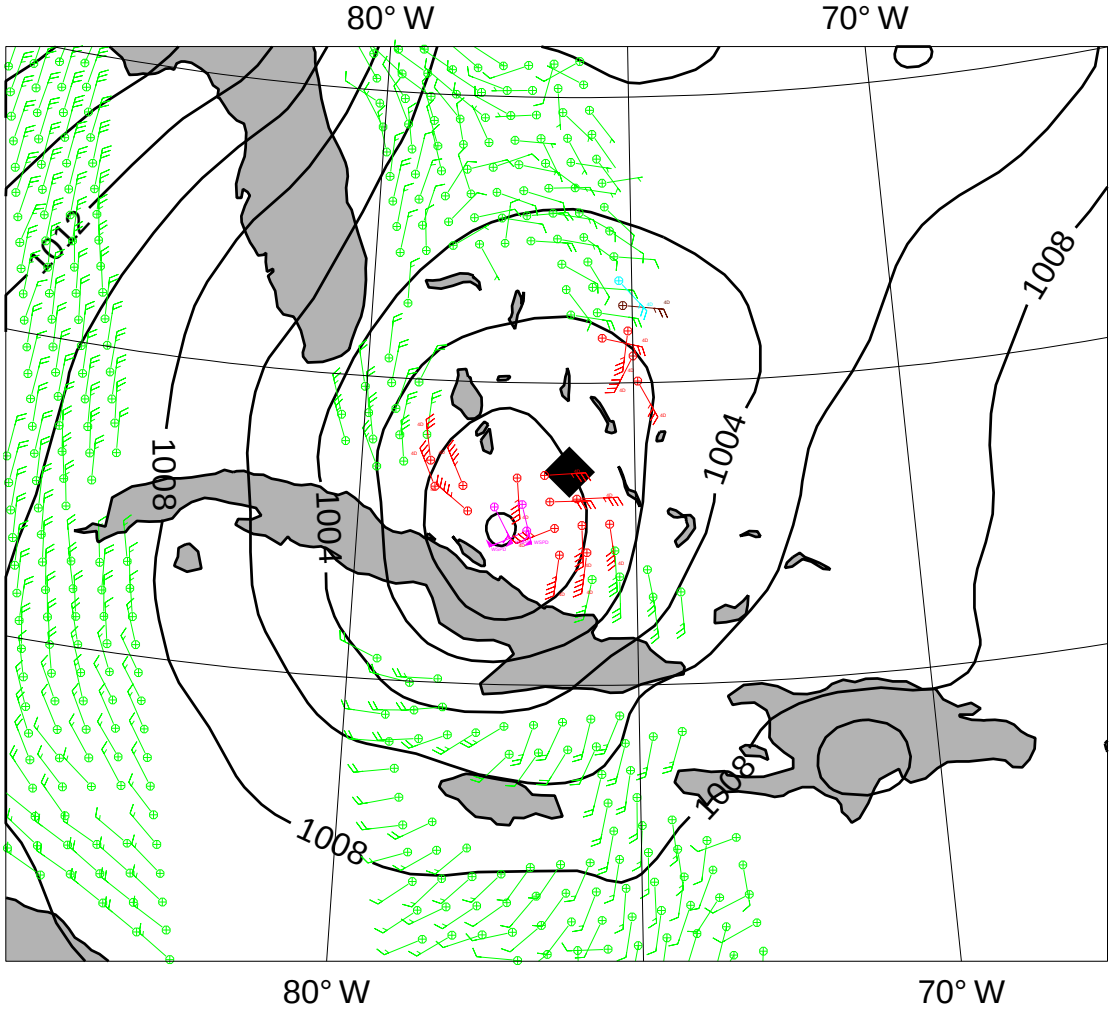

Figure 8: NSCAT winds in the vicinity of hurricane Lili, 0355 UTC 19 October 1996. The NSCAT ambiguity closest to the analyzed wind direction is plotted. MSLP analysis from NSCAT experiment valid at 0600 UTC 19 October 1996. Winds rejected by the variational quality control are red, magenta, or aqua.

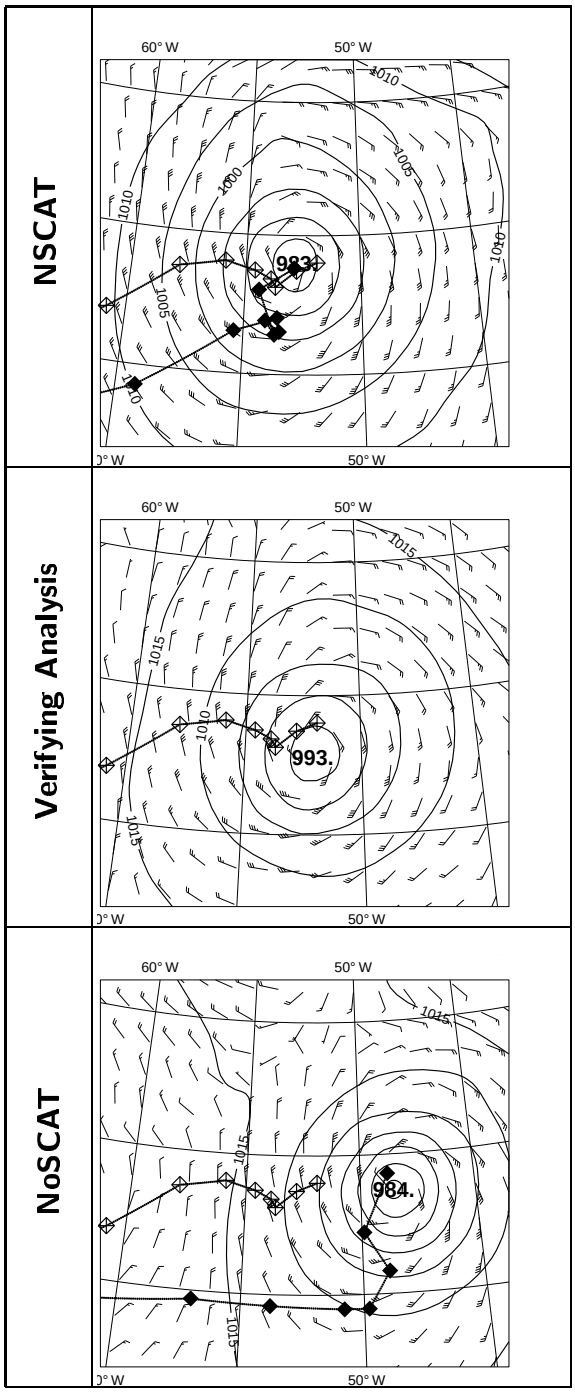

Figure 9: Forecasts of hurricane Lili valid at 1200 UTC 24 October 1996. Verifying analysis from ECMWF operational archive (middle panel) and 5-day forecasts of Lili's position from NSCAT (top panel) and NoSCAT (bottom panel). Observed 12-hourly positions of Lili until the verifying time are plotted in each panel with diamond-plus symbols. Forecast tracks of Lili in NSCAT and NoSCAT are plotted with filled diamonds. The observed central pressure and position from the NHC at 1200 UTC 24 October was 979 hPa at 34.0N and 51.9W. MSLP contour interval is 5 hPa.

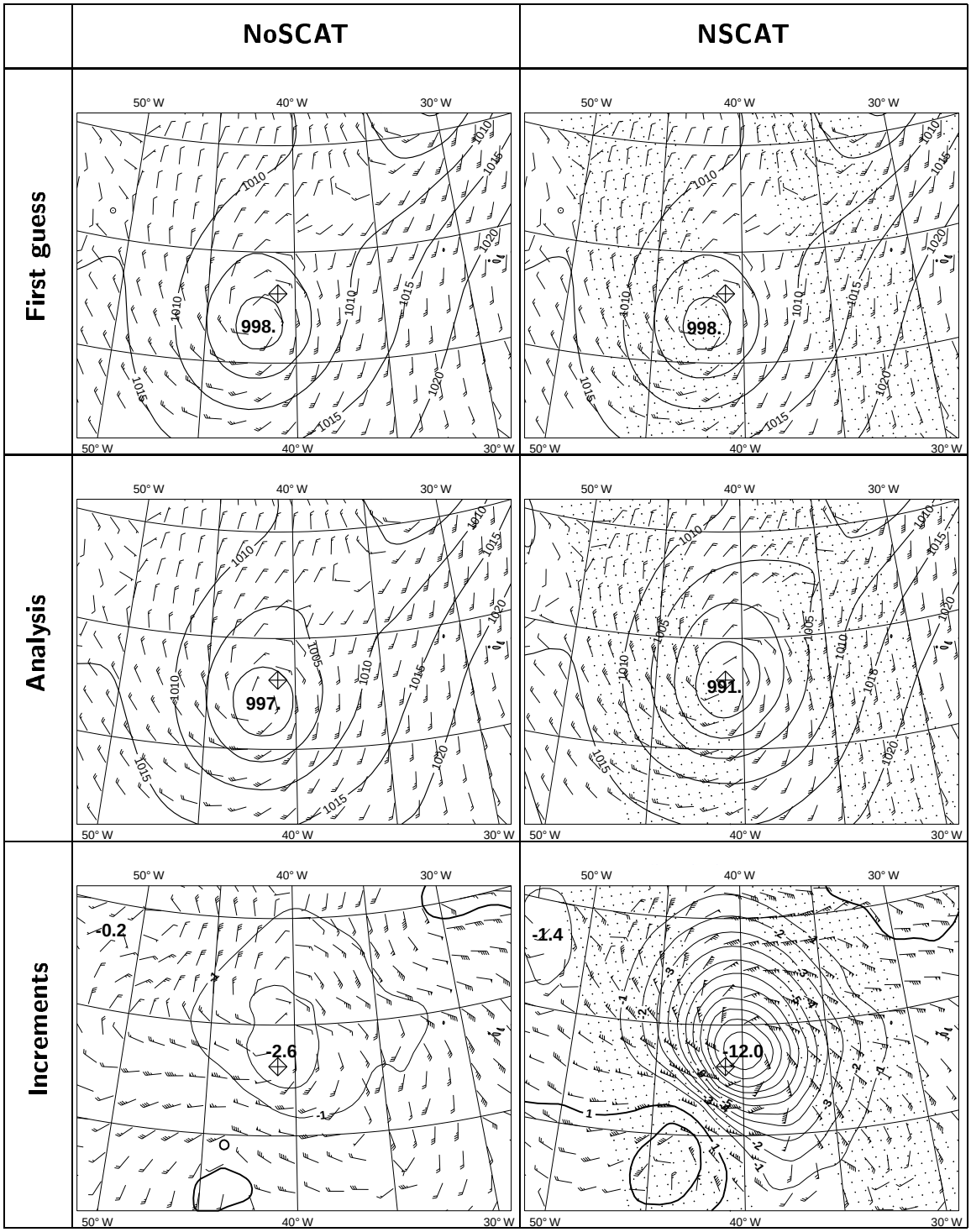

Figure 10: Analysis of hurricane Lili 0000 UTC 26 October 1996. Top panels are first guess 10 m wind (knots) and mean sea-level pressure (MSLP, hPa). Middle panels show analyzed wind and MSLP, and bottom panels show analysis increments of wind (times ten) and MSLP. The observed central pressure and position from the NHC at 0600 UTC 19 October was 975 hPa at 38.1N and 41.0W.

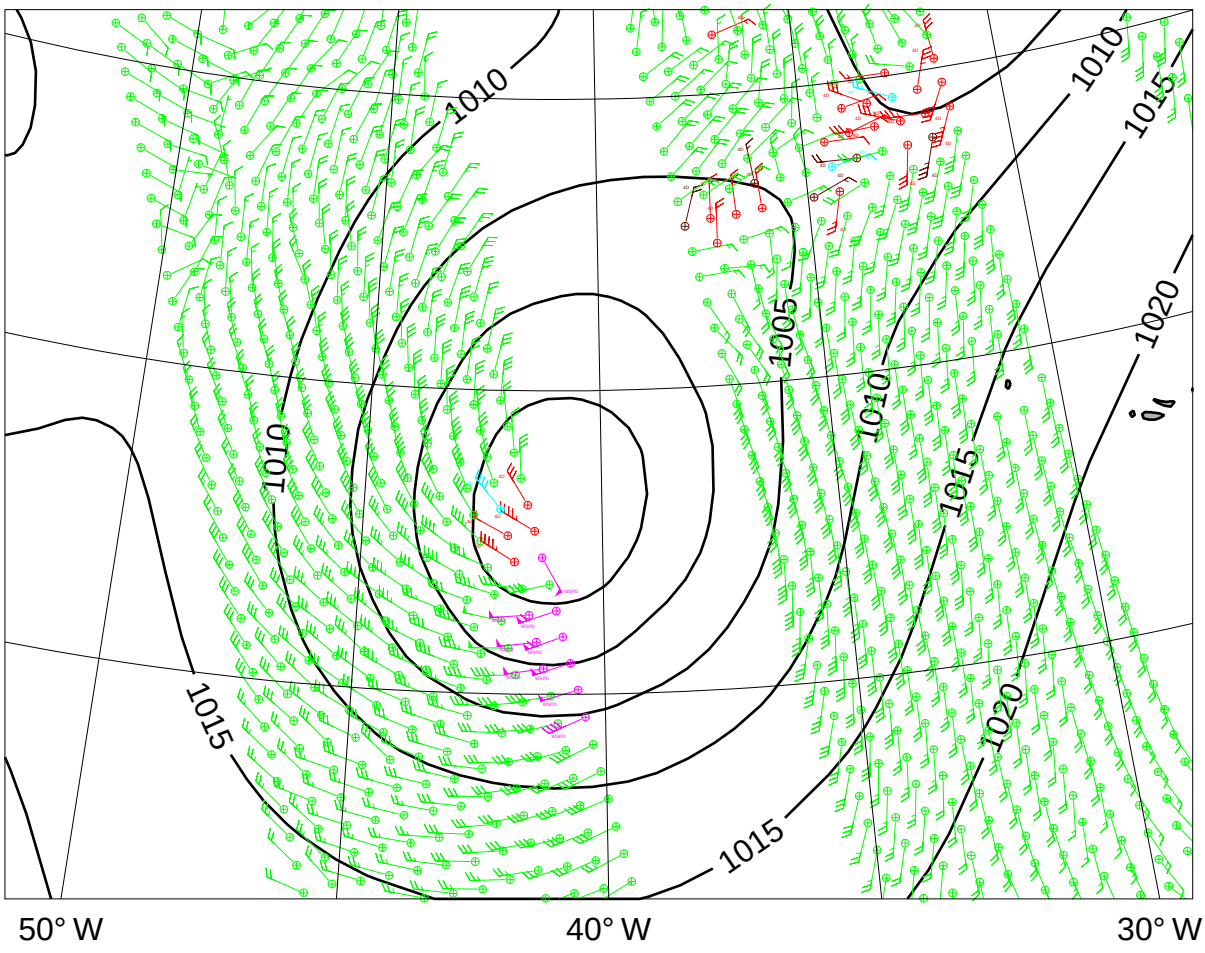

Figure 11: NSCAT winds in the vicinity of hurricane Lili, 0051 UTC 26 October 1996. The NSCAT ambiguity closest to the analyzed wind direction is plotted. MSLP analysis from NSCAT experiment valid at 0000 UTC 26 October 1996. Winds rejected by the variational quality control are red, magenta, or aqua.

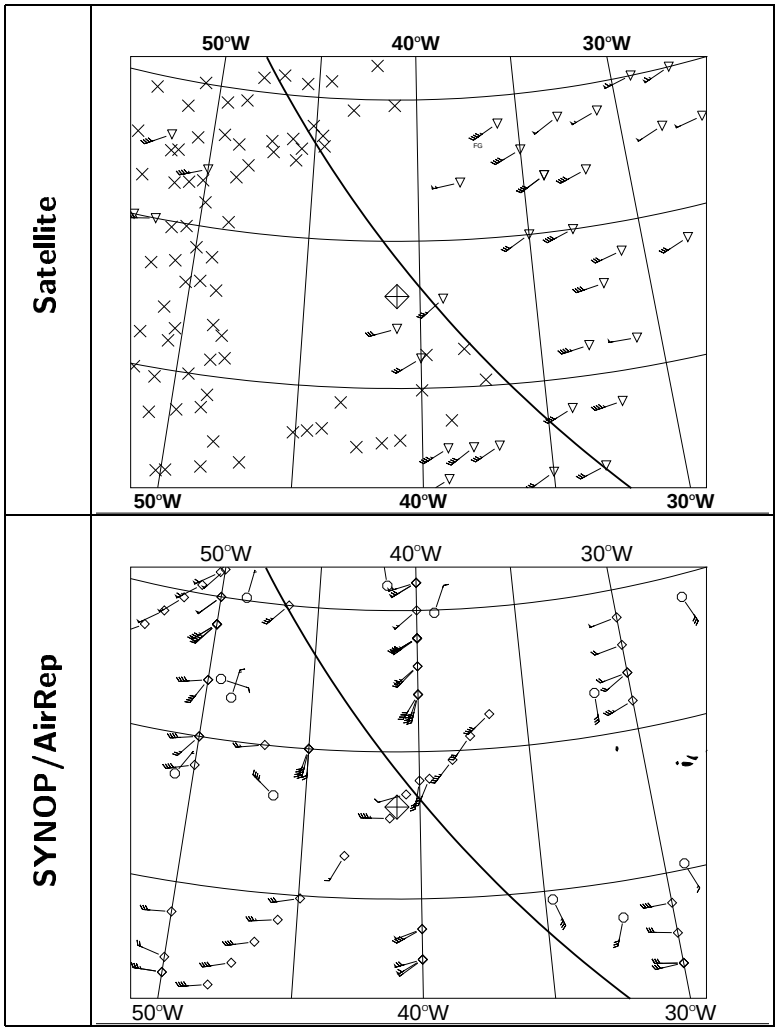

Figure 12: Non-NSCAT data presented to the analysis at 0000 UTC 26 October 1996: satellite data (upper panel; TOVS retrievals-crosses, satellite cloud motion winds-inverted triangles) and synoptic and aircraft reports (lower panel; synop/ship reports-circles, aircraft reports-diamonds). Hurricane Lili's observed position is marked in both panels. Each panel also has a cross section locator for Figs. 13–15 and Fig. 17.

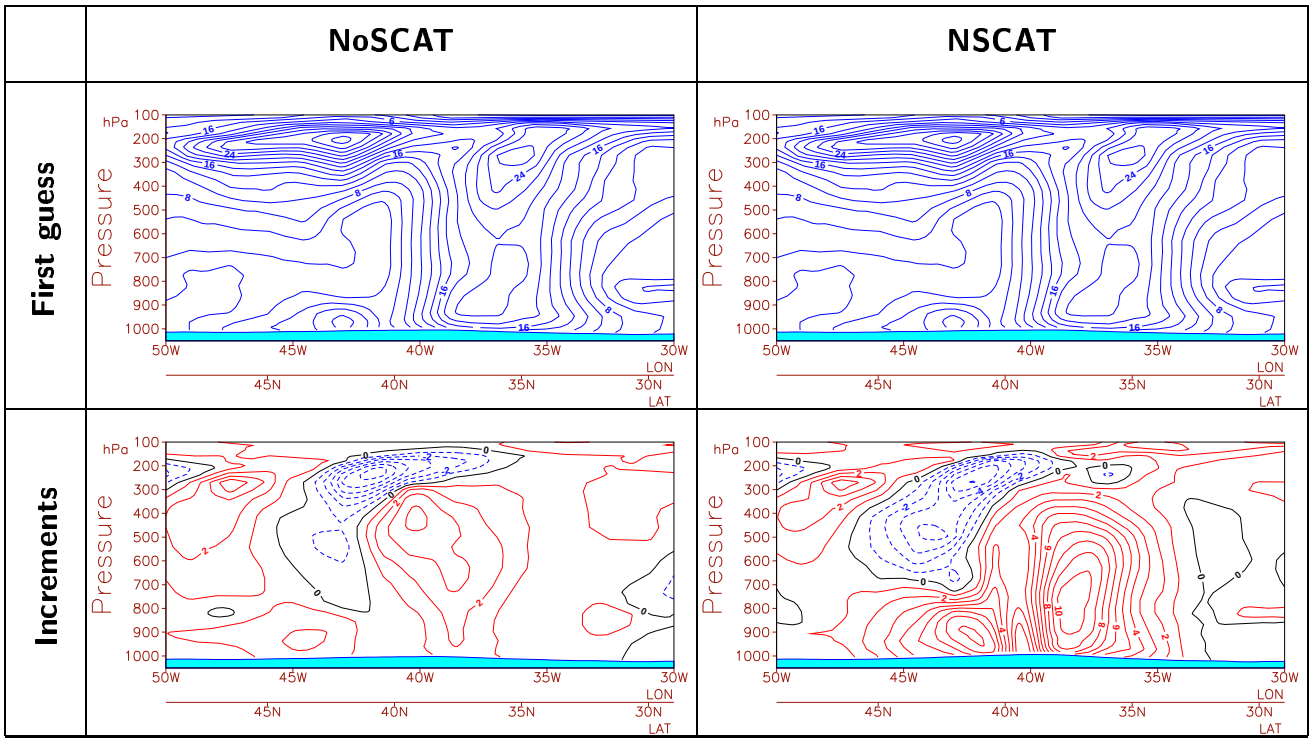

Figure 13: Cross sections of scalar wind speed valid 0000 UTC 26 October 1996: first guess wind speed (m/s) from NoSCAT and NSCAT (upper panels) and wind speed increments (m/s) from NoSCAT and NSCAT (lower panels). Cross section location is shown in Fig. 12.

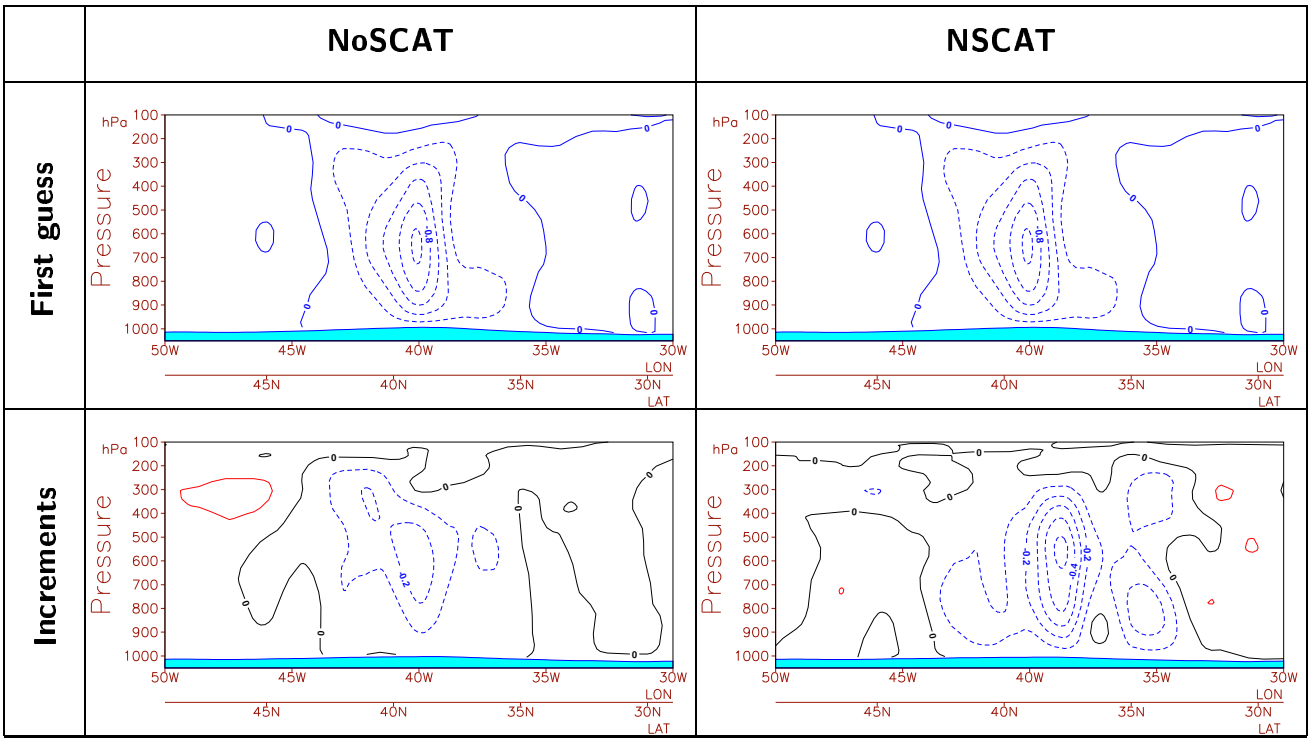

Figure 14: Cross sections of vertical velocity valid 0000 UTC 26 October 1996: first guess vertical velocity (Pa/s) from NoSCAT and NSCAT (upper panels) and vertical velocity increments (Pa/s) from NoSCAT and NSCAT (lower panels). Cross section location is shown in Fig. 12.

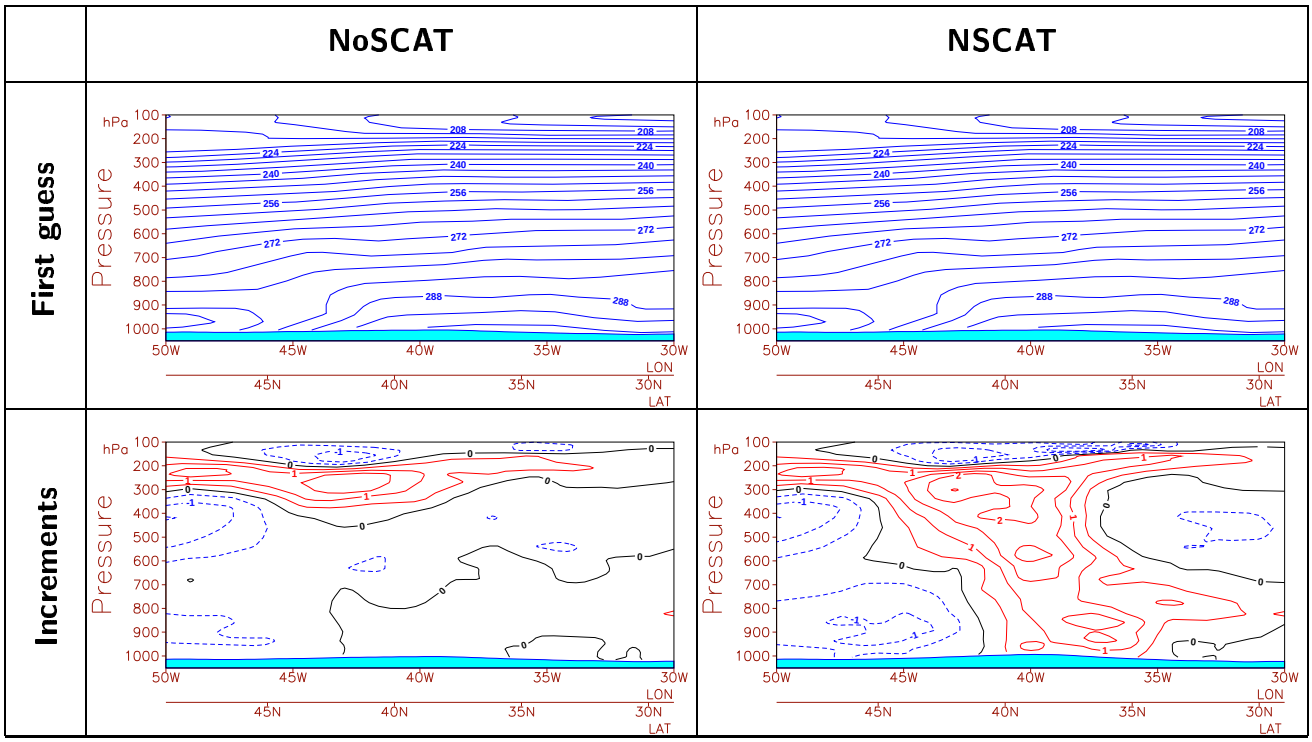

Figure 15: Cross sections of temperature valid 0000 UTC 26 October 1996: first guess temperature (K) from NoSCAT and NSCAT (upper panels) and temperature increments (°C) from NoSCAT and NSCAT (lower panels). Cross section location is shown in Fig. 12.

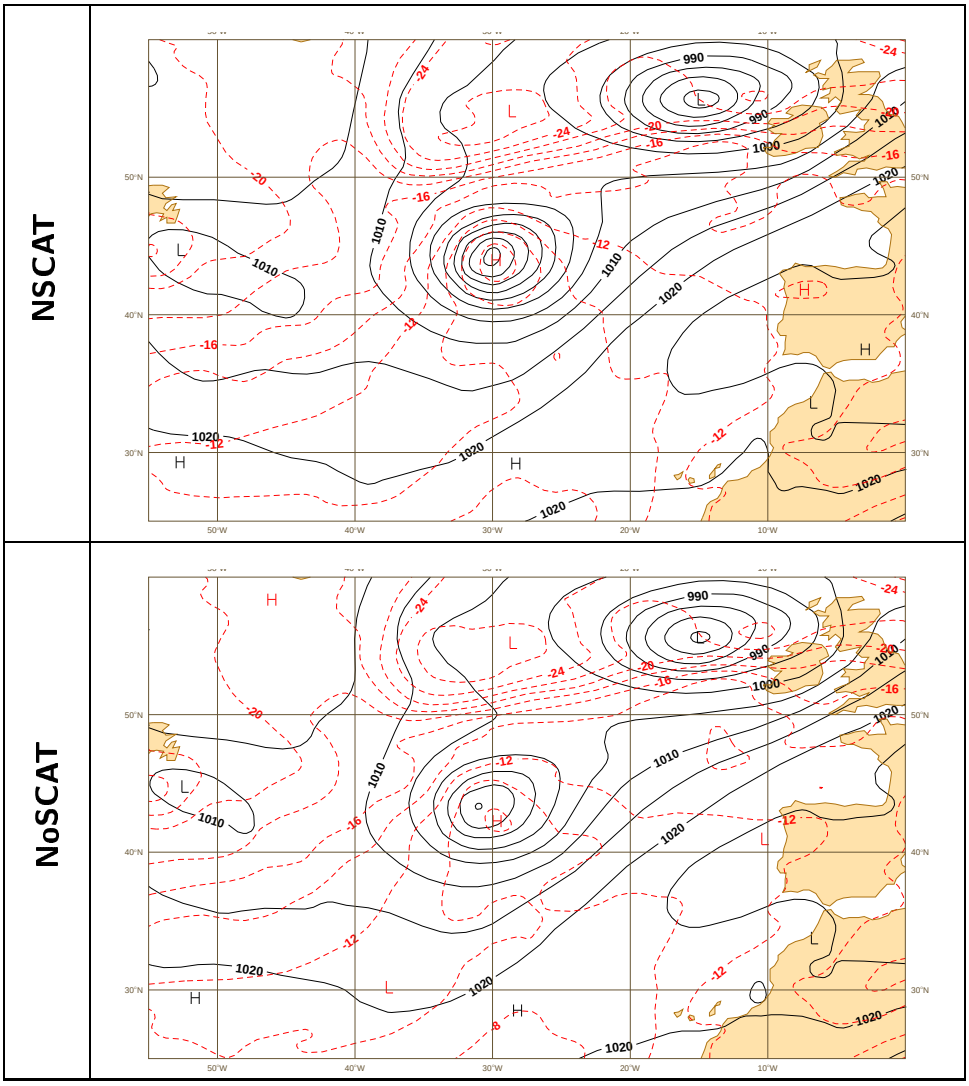

Figure 16: Comparison of NSCAT (upper panel) and NoSCAT (lower panel) MSLP and 500 hPa temperature (C) analyses valid 0000 UTC 27 October 1996.

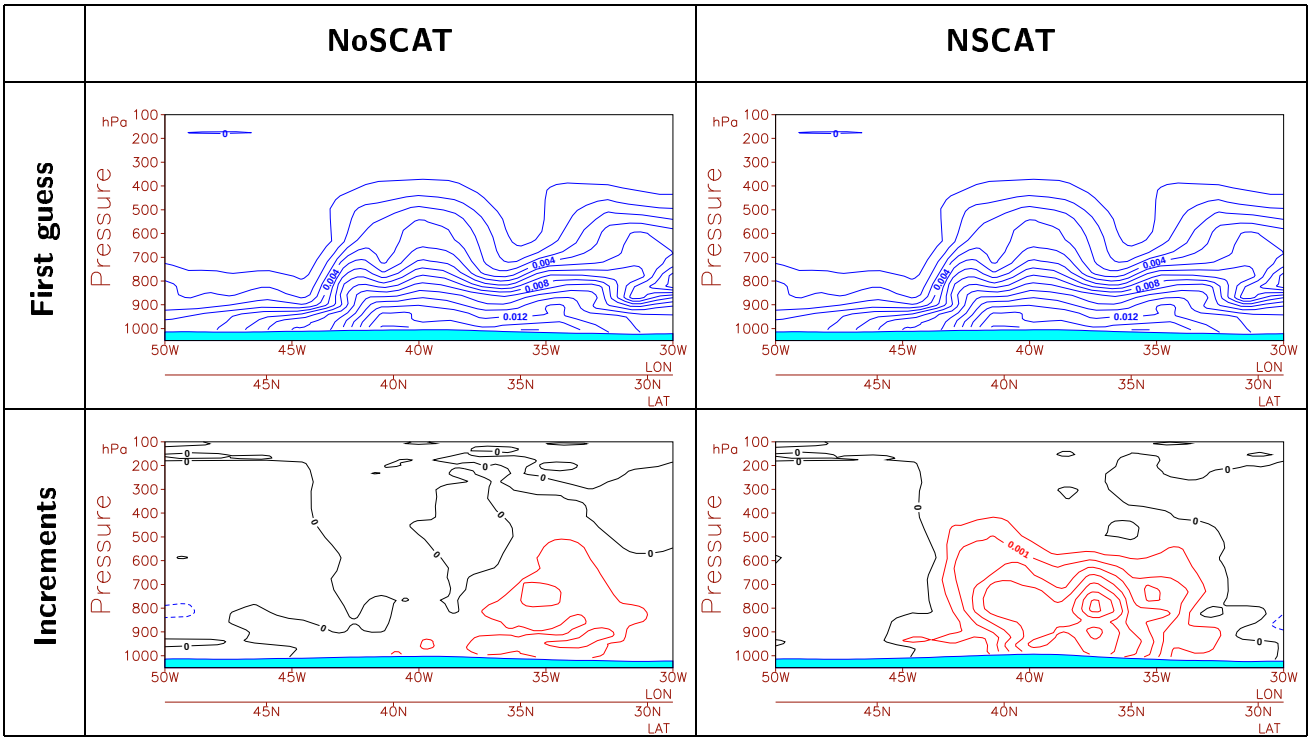

Figure 17: Cross sections of specific humidity valid 0000 UTC 26 October 1996: first guess specific humidity (kg/kg) from NoSCAT and NSCAT (upper panels) and specific humidity increments (kg/kg) from NoSCAT and NSCAT (lower panels). Cross section location is shown in Fig. 12.

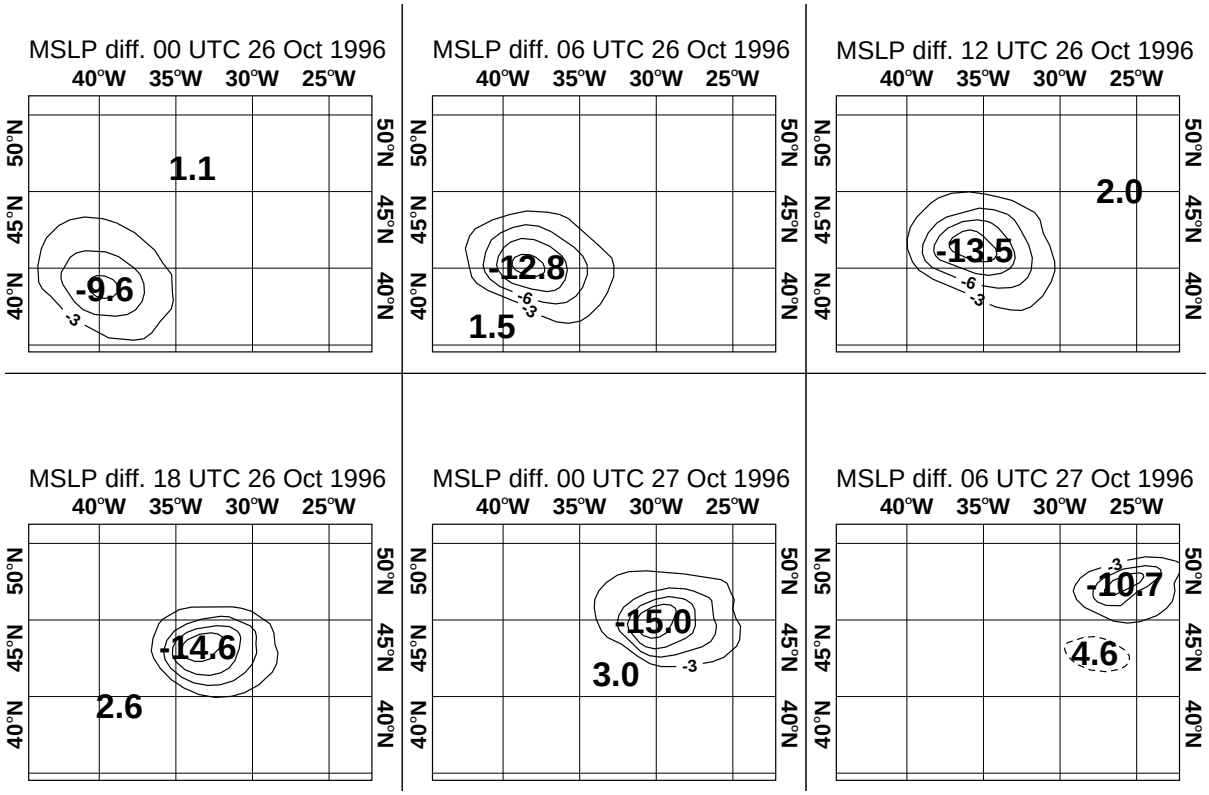

Figure 18: Analysis differences of MSLP (NSCAT-NoSCAT) for 6-hourly analyses, 0000 UTC 26 October - 0600 UTC 27 October 1996. The contour interval is 3 hPa. Maximum differences are displayed (units hPa).

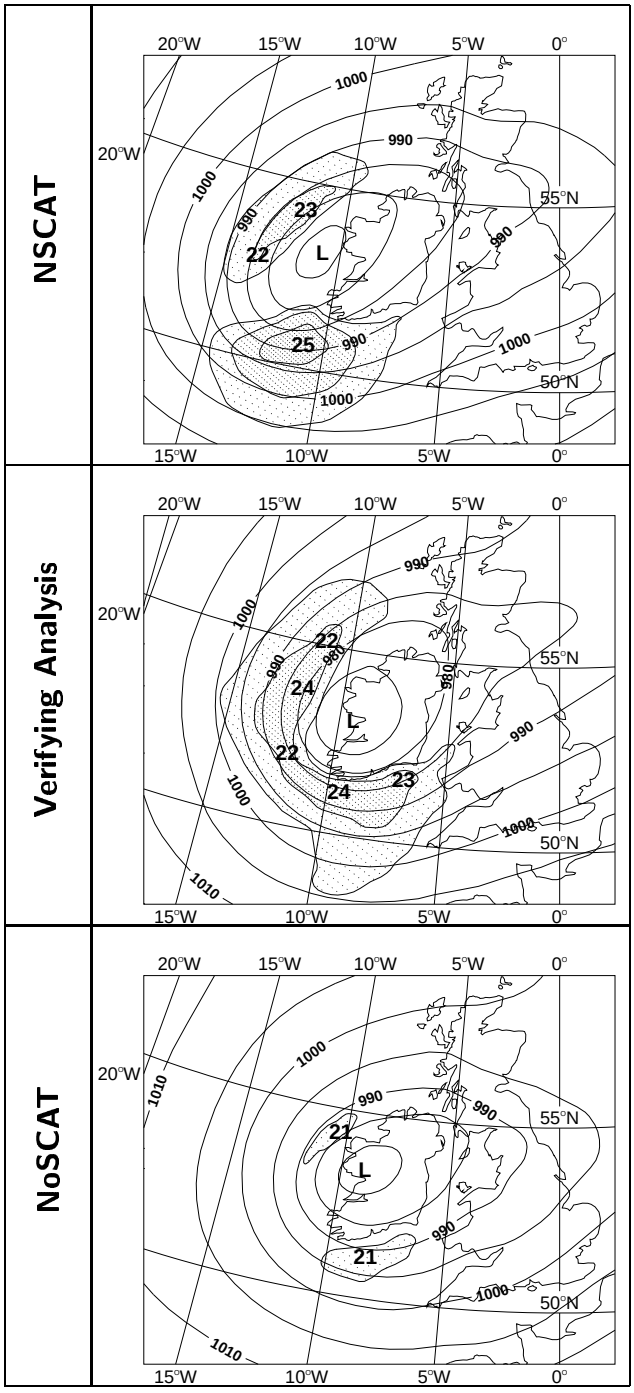

Figure 19: Forecasts of hurricane Lili valid 1200 UTC 28 October 1996: verifying analysis from the NoSCAT experiment (middle panel) and 2-day forecasts of Lili's position from NSCAT and NoSCAT (top and bottom panels, respectively). MSLP contour interval is 5 hPa, and wind speed is contoured every 2 m/s beginning at 20 m/s. The observed central pressure from the NHC at 1200 UTC 28 October was 970 hPa.

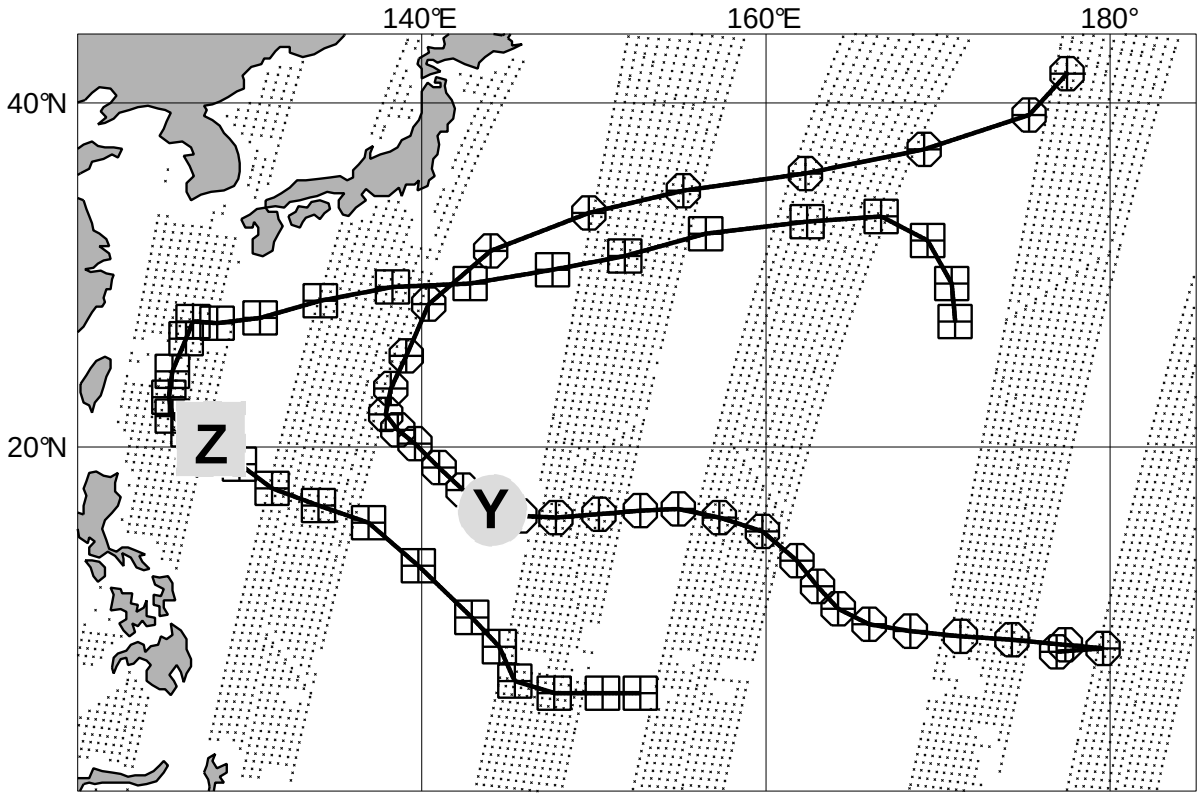

Figure 20: Tracks of typhoons Yates and Zane through the period 1200 UTC 17 September 1996 to 0000 UTC 06 October 1996. Observed positions at 0000 and 1200 UTC from the NHC are plotted as circle-plus (⊕) and box-plus symbols for Yates and Zane, respectively. Six hour NSCAT data coverage beginning at 2100 UTC 27 September 1996 is shown in fine dots. "Y" and "Z" mark the positions of Yates and Zane at 1200 UTC 26 September 1996, the time used as a case study in this paper.

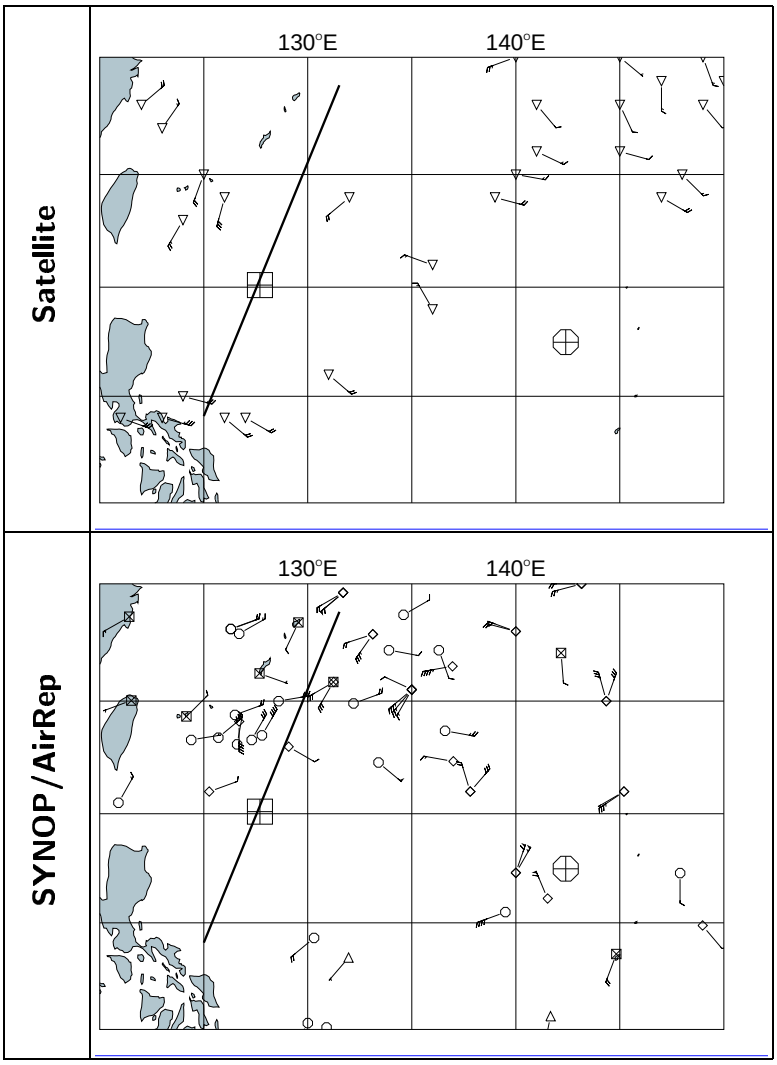

Figure 21: Non-NSCAT data presented to the analysis valid 1200 UTC 26 September 1996: satellite data (upper panel; satellite cloud motion winds-inverted triangles) and synoptic and aircraft reports (lower panel; synop/ship reports-circles, aircraft reports-diamonds, buoys-triangles, rawinsonde stations-small crossed squares). The positions of typhoons Yates and Zane are marked in both panels. Each panel also has a cross section locator for Figs. 28–31.

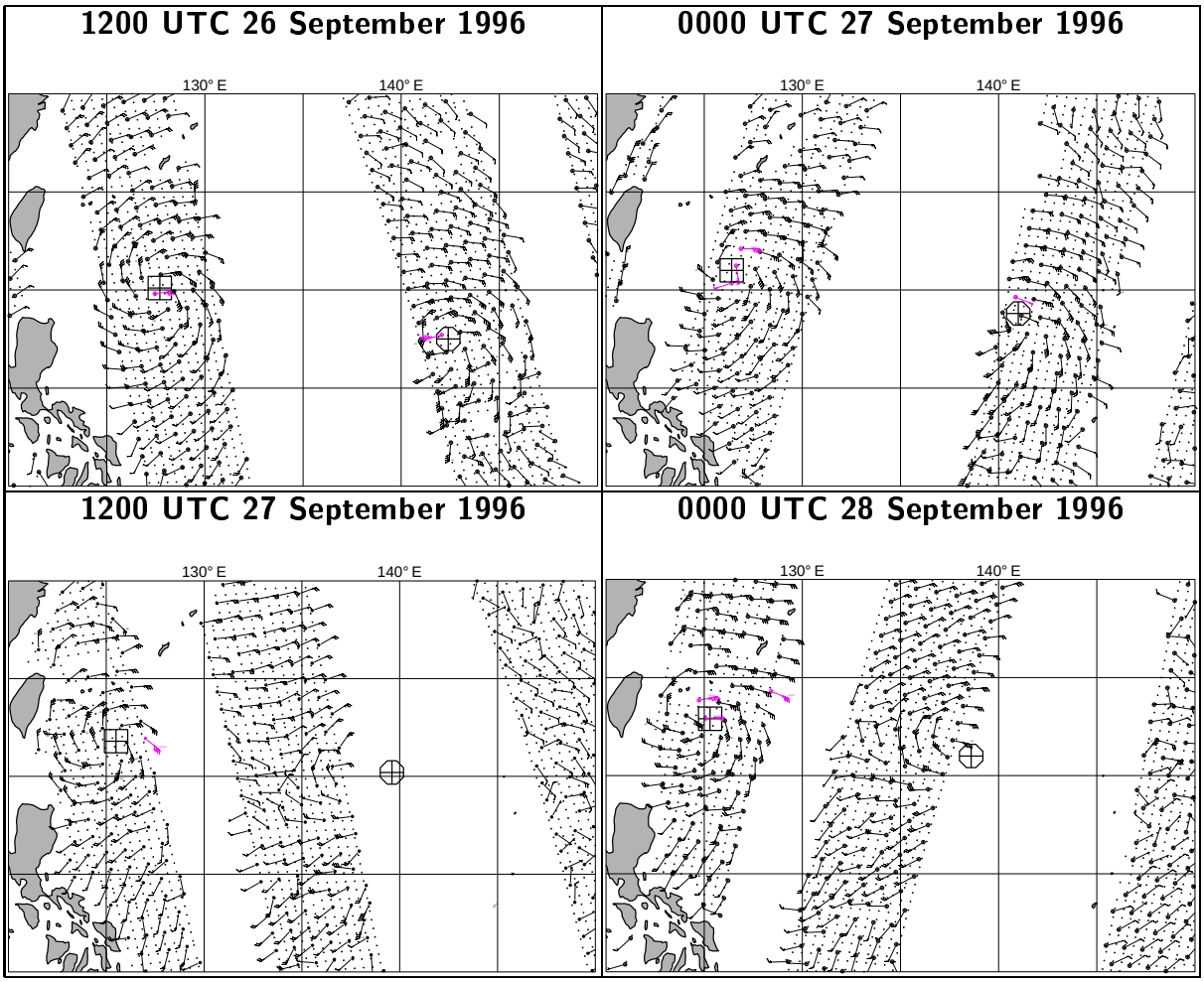

Figure 22: NSCAT data coverage in the region of typhoons Yates and Zane. These plots show data used in analyses valid 1200 UTC 26 September 1996 (upper left), 0000 UTC 27 September 1996 (upper right), 1200 UTC 27 September 1996 (lower left) and 0000 UTC 28 September 1996 (lower right). Data are thinned for plotting purposes. The full resolution of the data may be seen by the small dots.

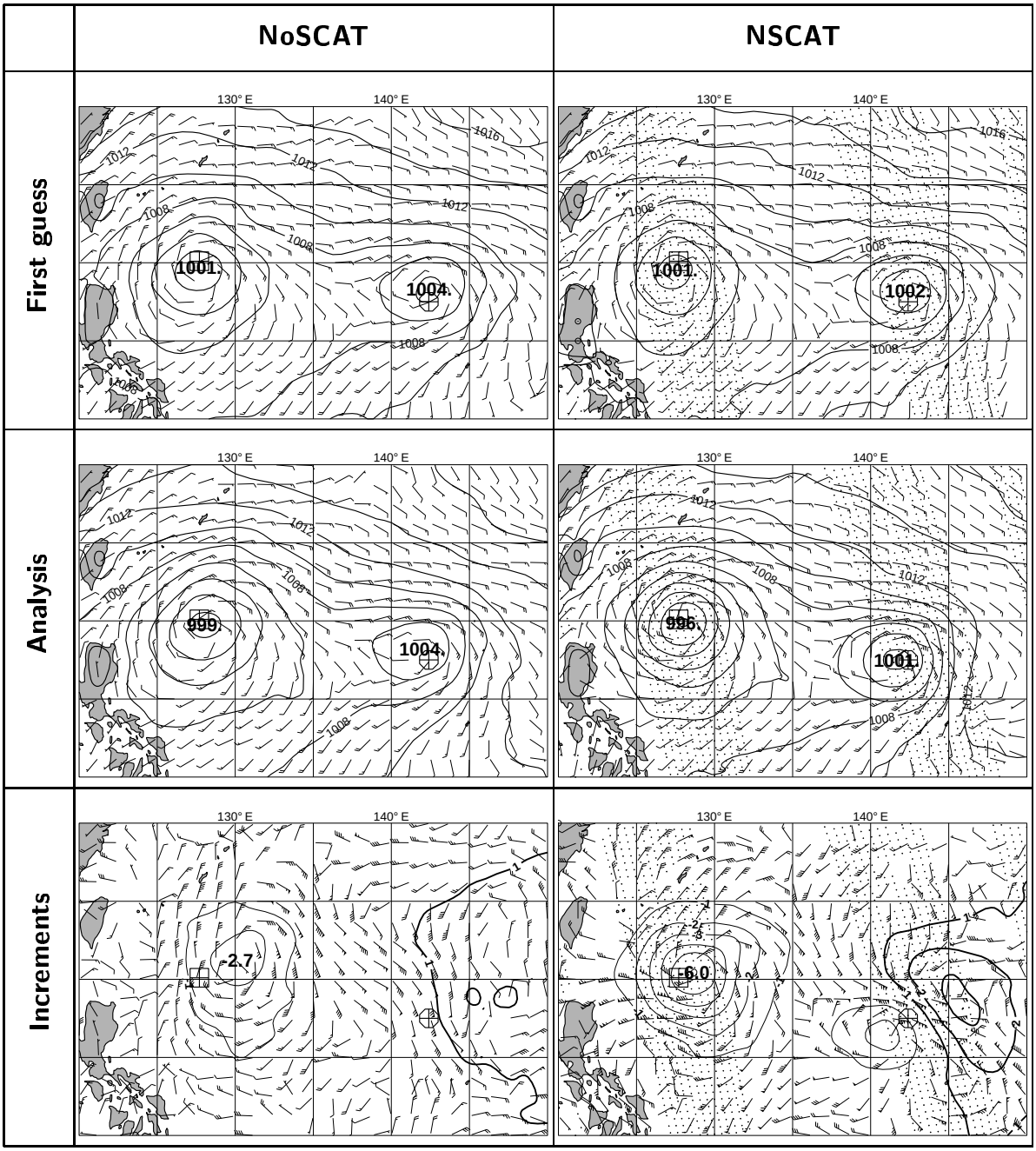

Figure 23: Analysis of typhoons Yates and Zane 1200 UTC 26 September 1996. Top panels are first guess 10 m wind (knots) and mean sea-level pressure (MSLP, hPa). Middle panels show analyzed wind and MSLP, and bottom panels show analysis increments of wind (times ten) and MSLP. At 1200 UTC 26 September, Yates was estimated to be a category 4 typhoon at 17.3N 142.4E, and Zane was estimated to be a category 3 typhoon at 20.1N and 127.7E. MSLP contour intervals are 2 hPa for first guess and analysis panels, and 1 hPa for increment panels.

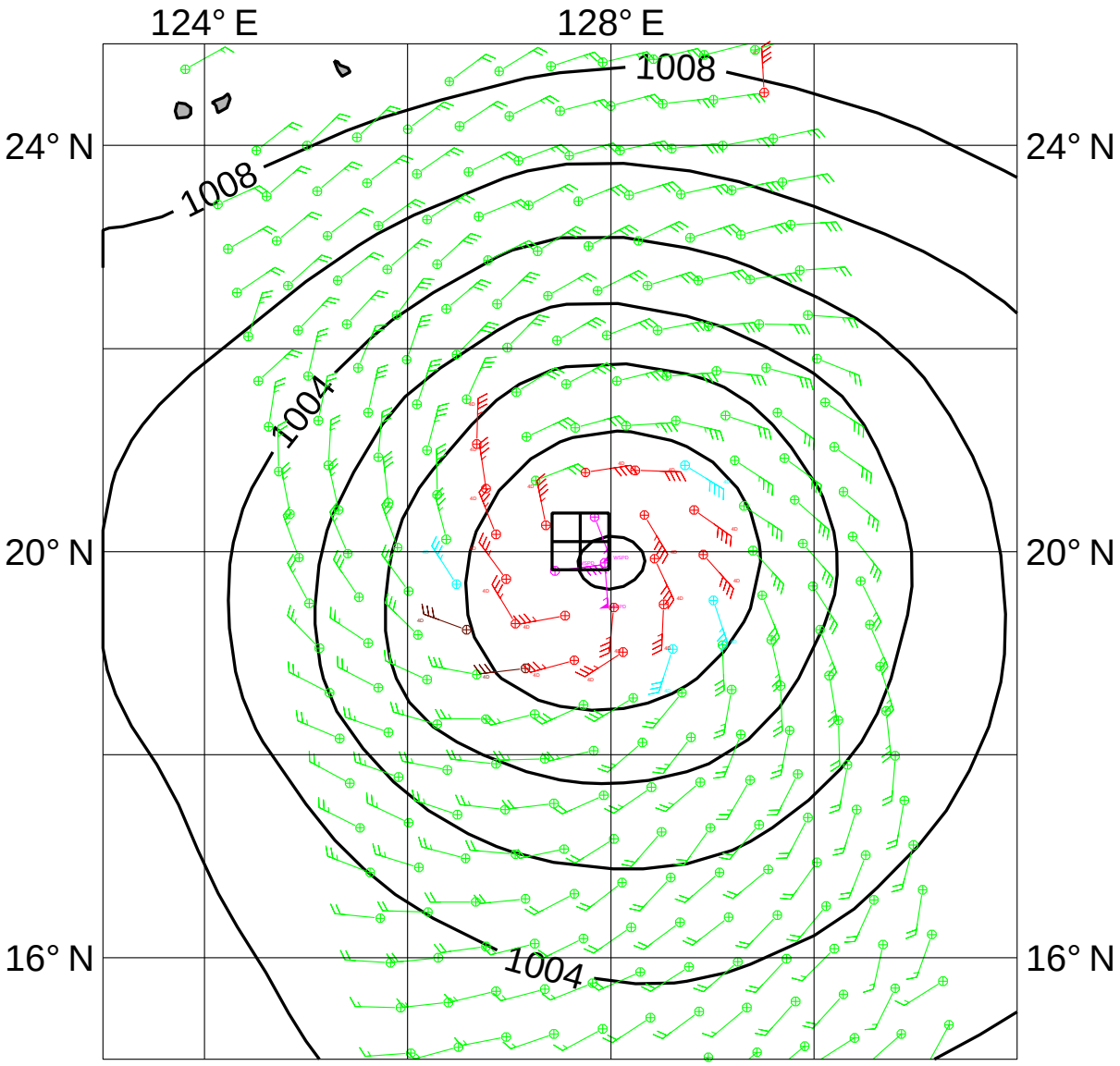

Figure 24: NSCAT winds in the vicinity of typhoon Zane, 1418 UTC 26 September 1996. The NSCAT ambiguity closest to the analyzed wind direction is plotted. MSLP analysis from NSCAT experiment valid at 1200 UTC 26 September 1996. Winds rejected by the variational quality control are red, magenta, or aqua.

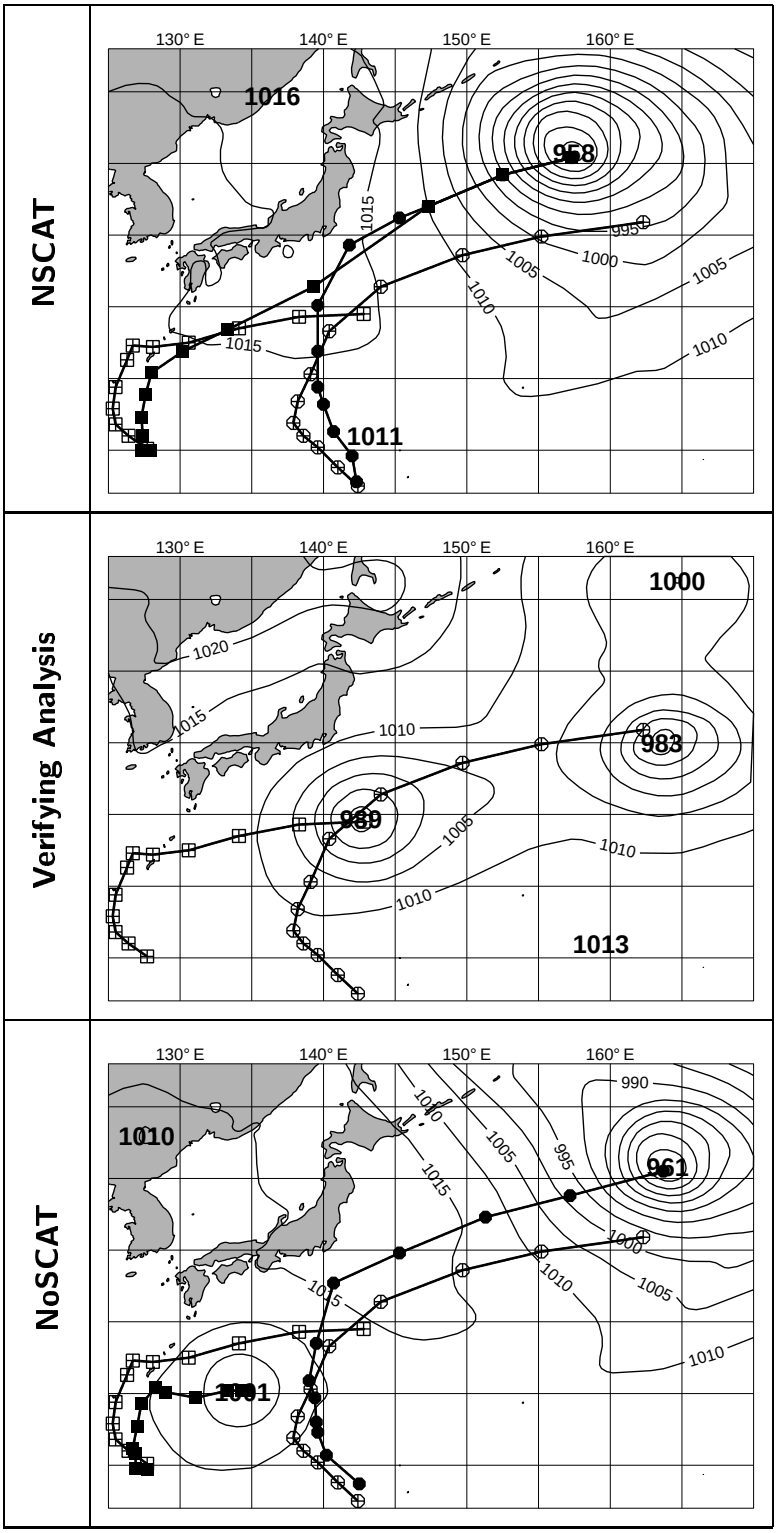

Figure 25: Forecasts of typhoons Yates and Zane valid at 0000 UTC 2 October 1996: verifying analysis from the NSCAT experiment (middle panel) and 5.5-day forecasts from NSCAT and NoSCAT (top and bottom panels, respectively). Observed or forecast 12-hourly positions of Yates and Zane are plotted in each panel as circle-plus and box-plus symbols, respectively. Forecast tracks of are plotted with filled circles and squares. MSLP contour interval is 5 hPa.

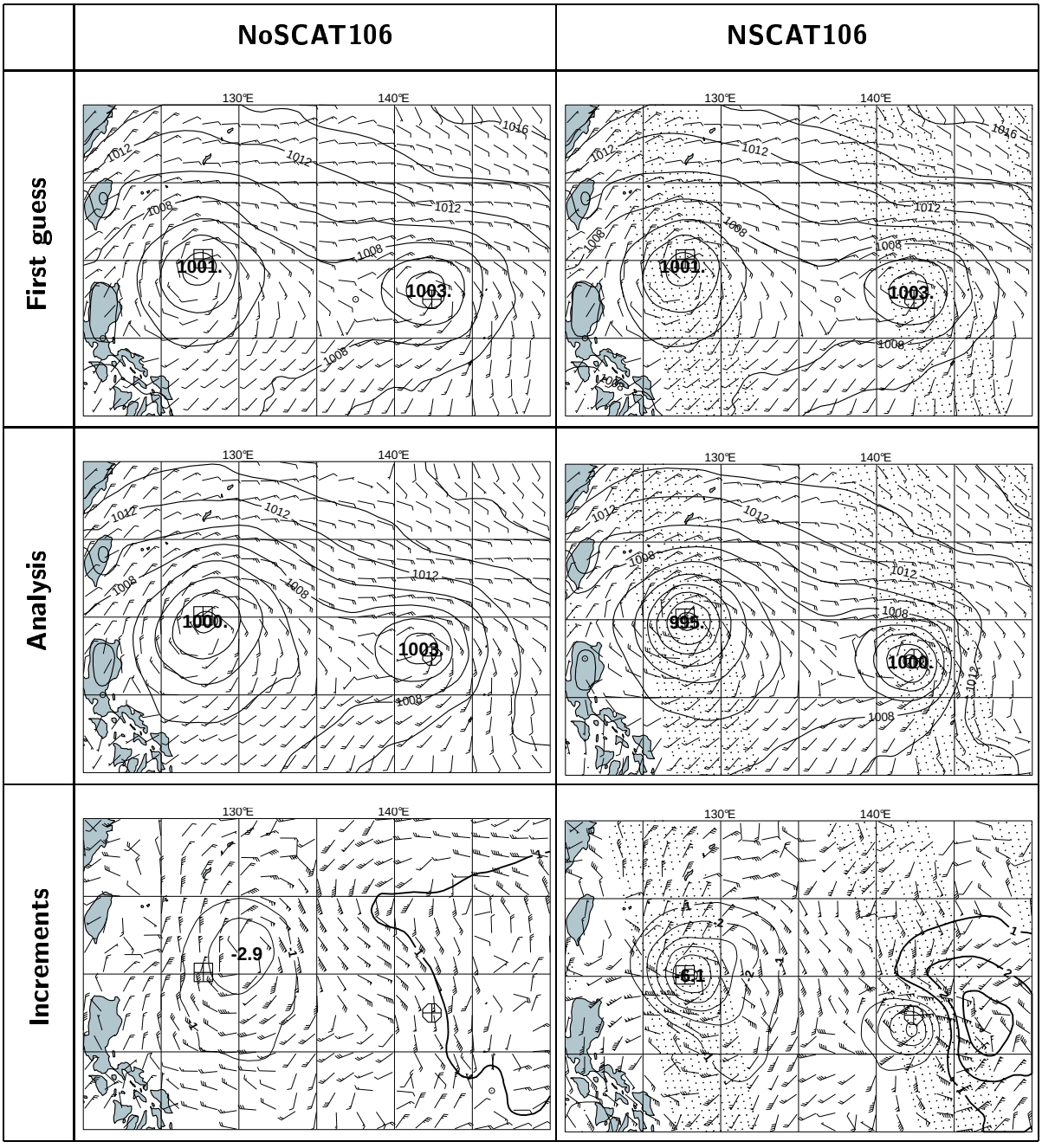

Figure 26: Same as Fig. 23 but for the T106 analyses.

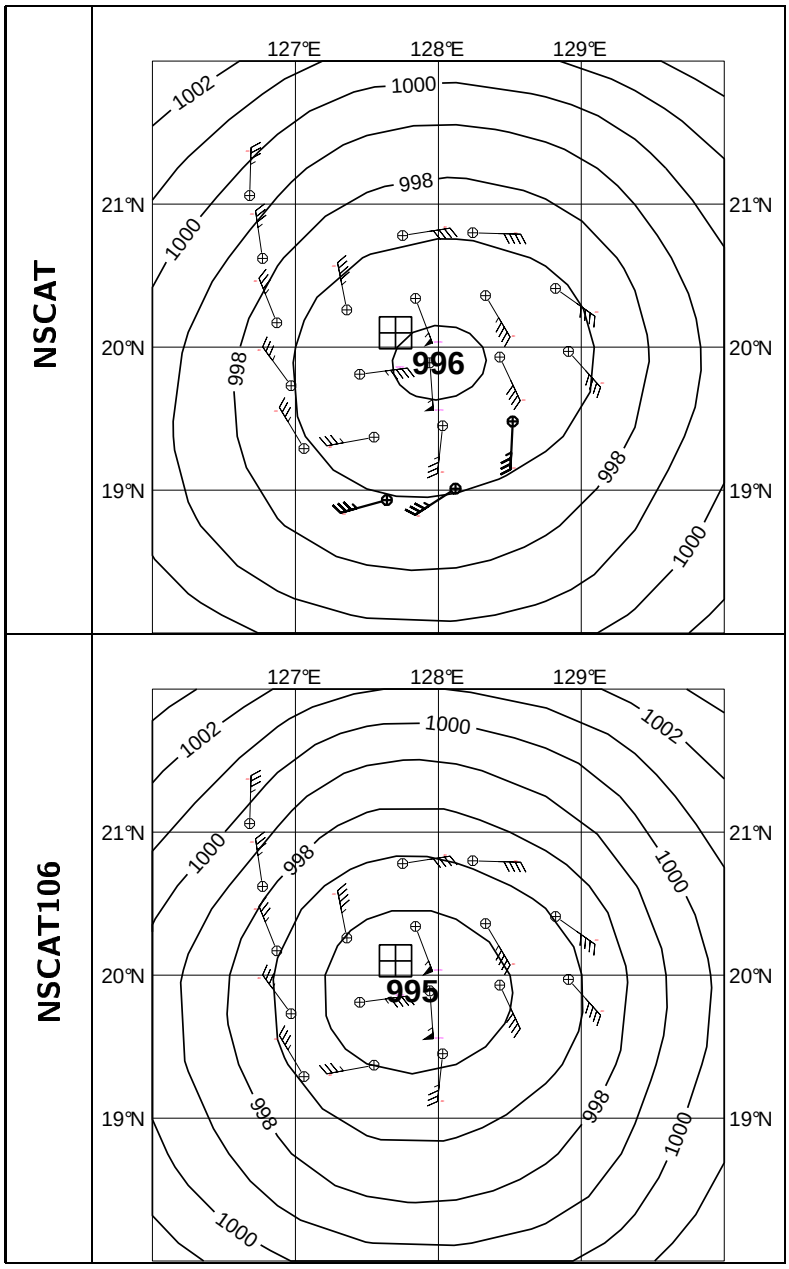

Figure 27: NSCAT data rejected by 4D-Var quality control from the analysis for typhoon Zane, 1200 UTC 26 September 1996, from experiements NSCAT (upper panel) and NSCAT106 (lower panel). Three observations rejected in the NSCAT analysis but used in the NSCAT106 analysis are highlighted in the upper panel. Winds rejected by the variational quality control in T63, but used in T106 are located to the south and southeast.

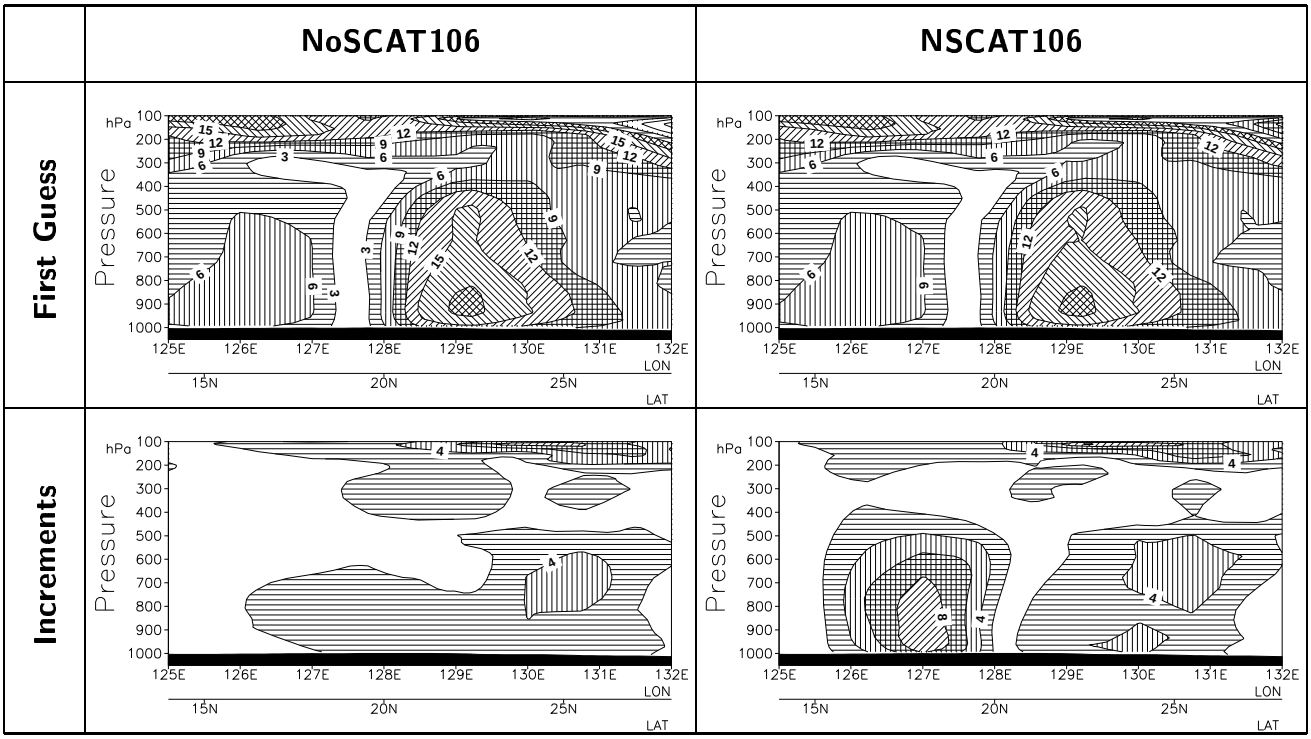

Figure 28: Cross sections of scalar wind speed valid 1200 UTC 26 September 1996 through typhoon Zane: first guess winds (m/s) from NoSCAT106 and NSCAT106 (upper panels) and wind speed increments (m/s) from NoSCAT106 and NSCAT106 (lower panels). Cross section location is shown in Fig. 21.

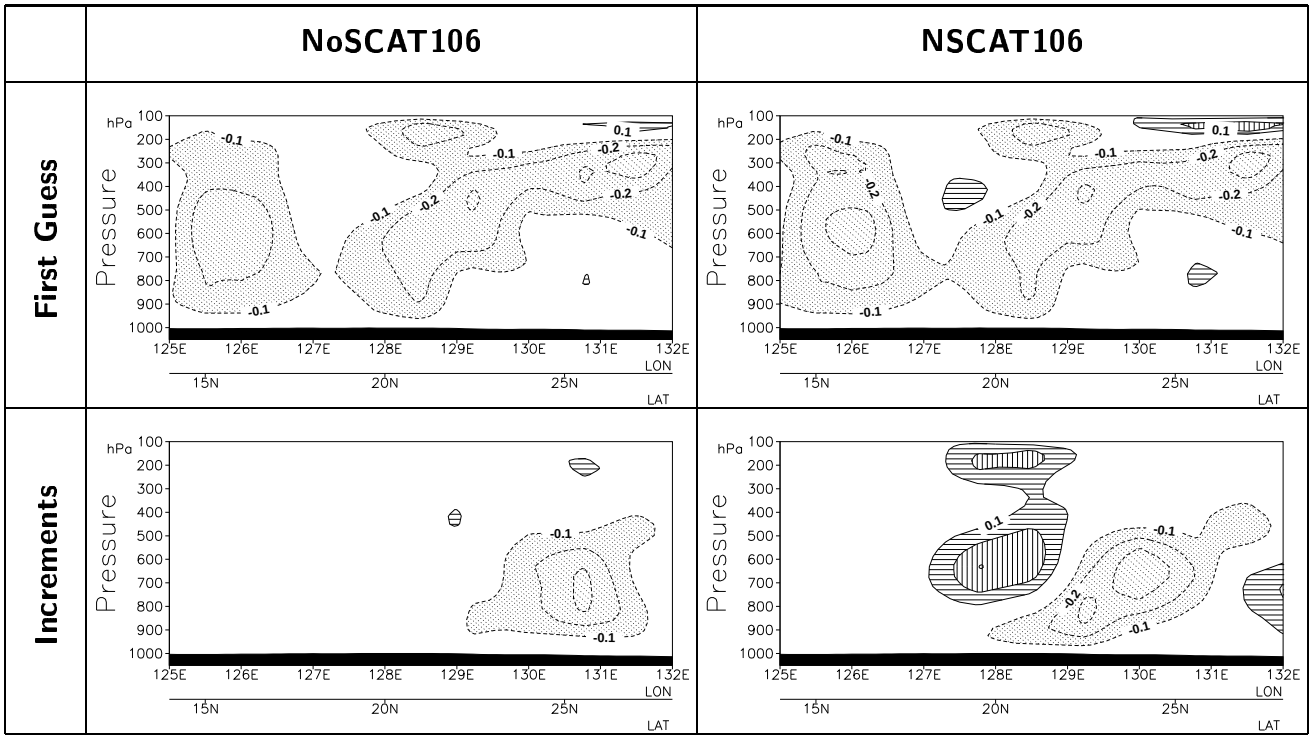

Figure 29: Cross sections of vertical velocity valid 1200 UTC 26 September 1996 through typhoon Zane: first guess vertical velocity (Pa/s) from NoSCAT106 and NSCAT106 (upper panels) and vertical velocity increments (Pa/s) from NoSCAT106 and NSCAT106 (lower panels). Cross section location is shown in Fig. 21.

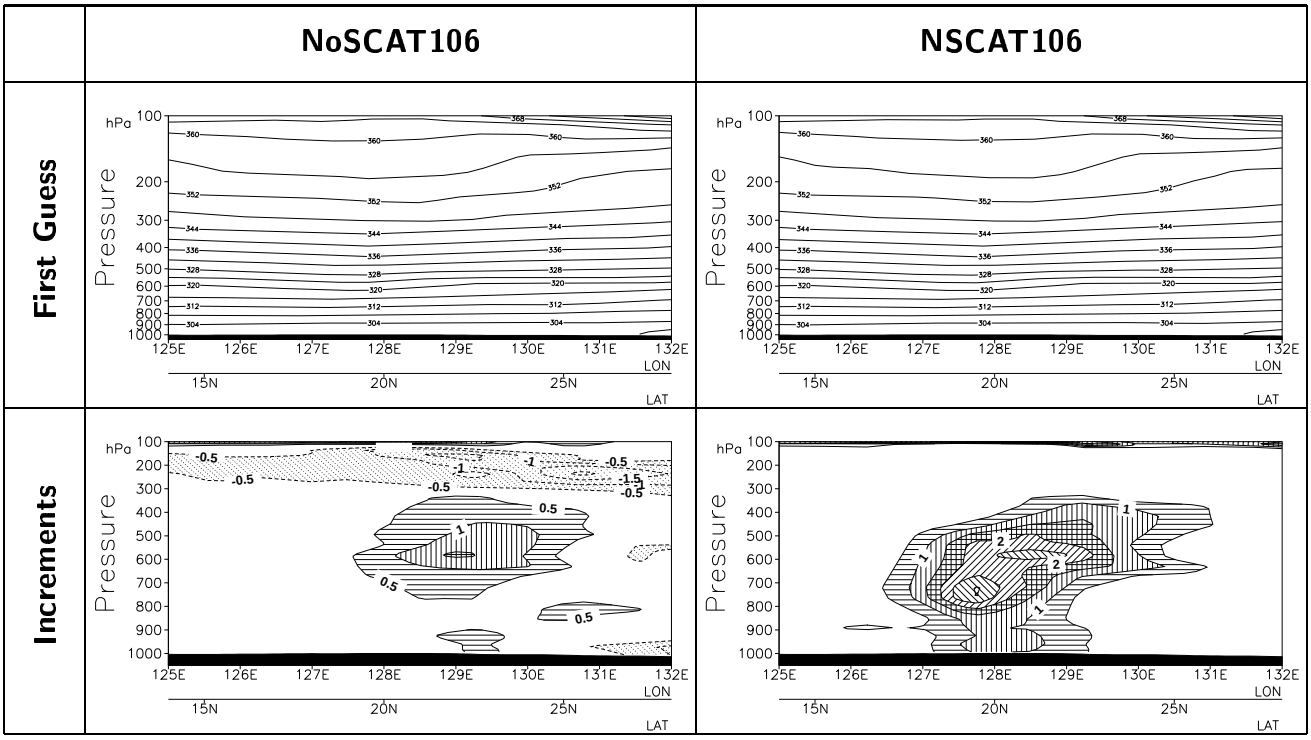

Figure 30: Cross sections of potential temperature valid 1200 UTC 26 September 1996 through typhoon Zane: first guess potential temperature (K) from NoSCAT106 and NSCAT106 (upper panels) and potential temperature increments (°C) from NoSCAT106 and NSCAT106 (lower panels). Cross section location is shown in Fig. 21.

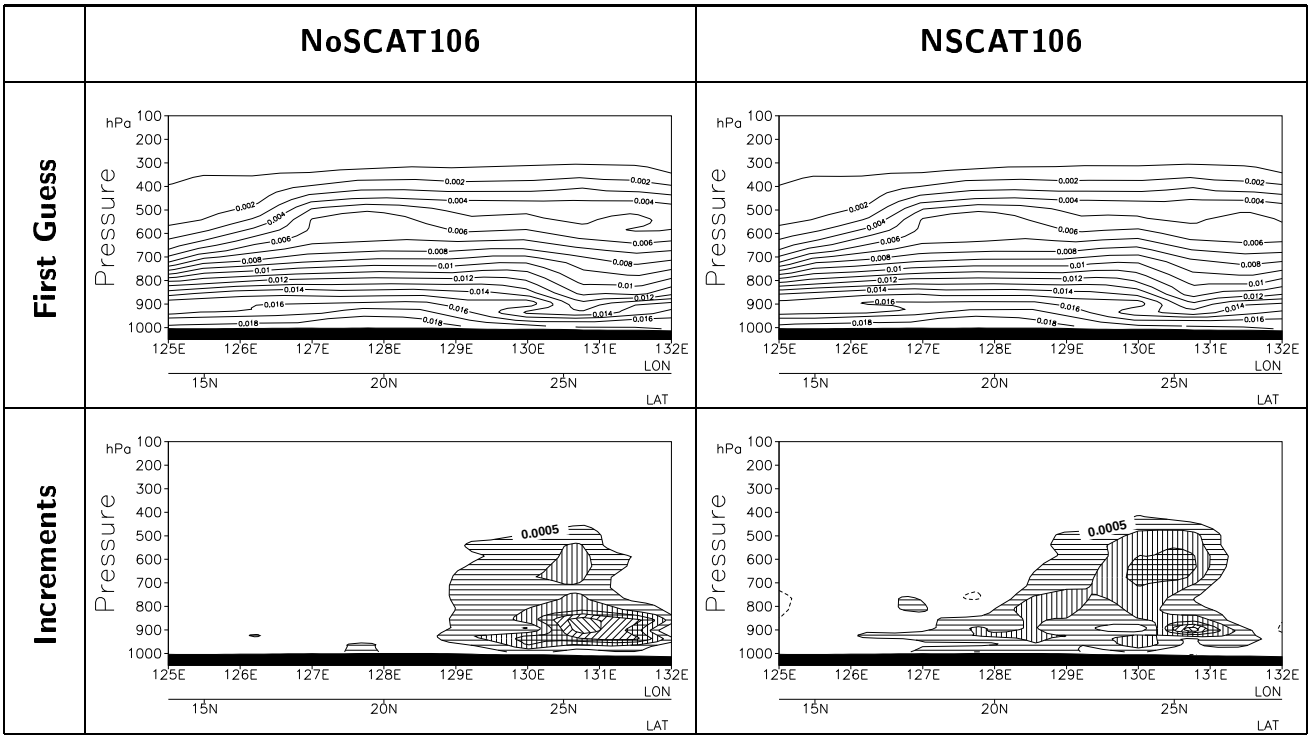

Figure 31: Cross sections of specific humidity valid 1200 UTC 26 September 1996 through typhoon Zane: first guess specific humidity (kg/kg) from NoSCAT106 and NSCAT106 (upper panels) and specific humidity increments (kg/kg) from NoSCAT106 and NSCAT106 (lower panels). Cross section location is shown in Fig. 21.

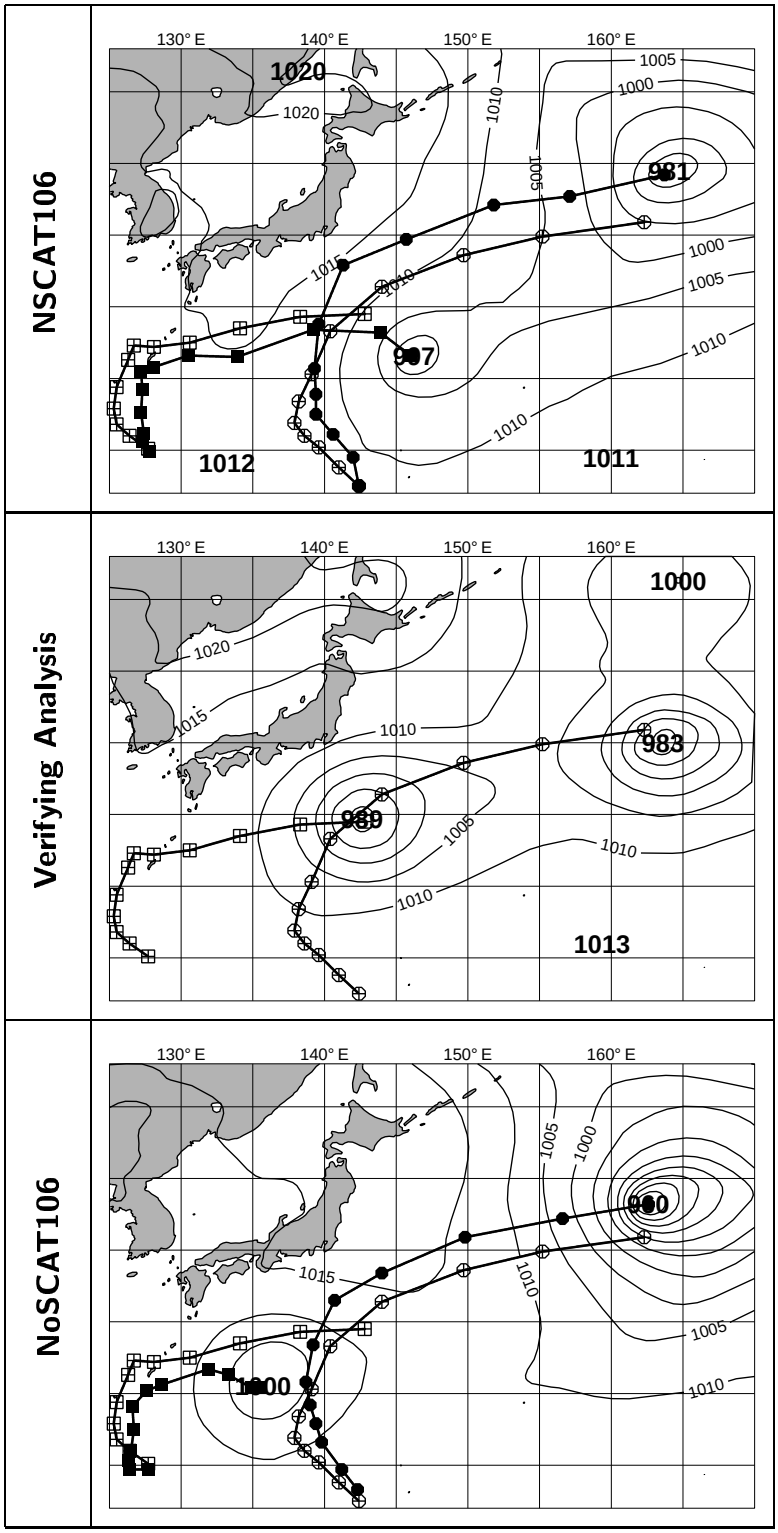

Figure 32: Forecasts of typhoons Yates and Zane valid 0000 UTC 3 October 1996: verifying analysis (middle panel) and 5.5-day forecasts from NSCAT106 and NoSCAT106 (top and bottom panels, respectively). Observed or forecast 12-hourly positions of Yates and Zane are plotted in each panel as circle-plus and box-plus symbols, respectively. Forecast tracks of are plotted with filled circles and squares. MSLP contour interval is 5 hPa.

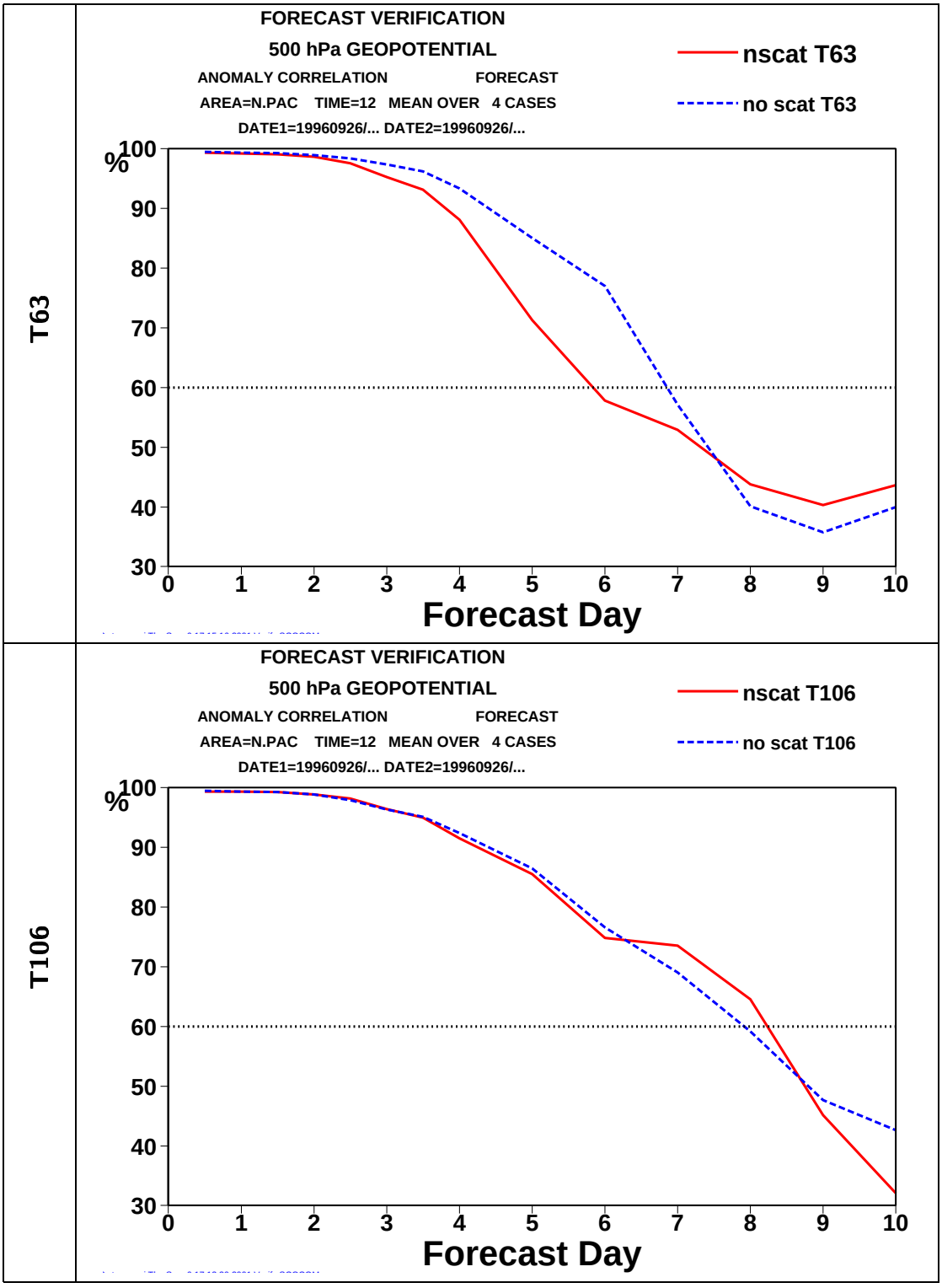

Figure 33: 500 hPa anomaly correlation forecast scores for the North Pacific region. Results shown are an average of four cases in September 1996. The upper panel compares NoSCAT with NSCAT (T63 resolution) while the lower panel compares NoSCAT106 with NSCAT106. The large impact of NSCAT106 is due to importance of treating typhoons Yates and Zane correctly by the assimilation system. In general, a smaller impact of NSCAT data would be expected than is seen in this case study.